



## RESEARCH ARTICLE

10.1029/2022JF006705

### Key Points:

- Ultra-high resolution time-lapse mapping is combined with flow monitoring and sediment cores to document submarine canyon activity
- Fast turbidity currents fail to cause notable bedform migration, though flows with similar speeds cause significant migration up-canyon
- Sub-meter to meter-scale scours, likely carved by internal tides, approach the scale of features preserved in the rock record

### Supporting Information:

Supporting Information may be found in the online version of this article.

### Correspondence to:

M. Wolfson-Schwehr,  
[monica.schwehr@gmail.com](mailto:monica.schwehr@gmail.com)

### Citation:

Wolfson-Schwehr, M., Paull, C. K., Caress, D. W., Gwiazda, R., Nieminski, N. M., Talling, P. J., et al. (2023). Time-lapse Seafloor surveys reveal how turbidity currents and internal tides in Monterey Canyon interact with the seabed at centimeter-scale. *Journal of Geophysical Research: Earth Surface*, 128, e2022JF006705. <https://doi.org/10.1029/2022JF006705>

Received 14 APR 2022

Accepted 28 MAR 2023

© 2023. The Authors.

This is an open access article under the terms of the [Creative Commons Attribution License](https://creativecommons.org/licenses/by/4.0/), which permits use, distribution and reproduction in any medium, provided the original work is properly cited.

# Time-Lapse Seafloor Surveys Reveal How Turbidity Currents and Internal Tides in Monterey Canyon Interact With the Seabed at Centimeter-Scale

M. Wolfson-Schwehr<sup>1,2</sup> , C. K. Paull<sup>1</sup>, D. W. Caress<sup>1</sup> , R. Gwiazda<sup>1</sup> , N. M. Nieminski<sup>3</sup> , P. J. Talling<sup>4</sup> , C. Carvajal<sup>1,5</sup>, S. Simmons<sup>6</sup> , and G. Troni<sup>1,7</sup> 

<sup>1</sup>Monterey Bay Aquarium Research Institute, Moss Landing, CA, USA, <sup>2</sup>Now at University of New Hampshire, Center for Coastal and Ocean Mapping, Durham, NH, USA, <sup>3</sup>U.S. Geological Survey, Pacific Coastal and Marine Science Center, Santa Cruz, CA, USA, <sup>4</sup>Departments of Geography and Earth Sciences, Durham University, Durham, UK, <sup>5</sup>Now at ConocoPhillips, Houston, TX, USA, <sup>6</sup>University of Hull, Energy and Environment Institute, Hull, UK, <sup>7</sup>Departamento de Ingeniería Mecánica y Metalúrgica, Pontificia Universidad Católica de Chile, Santiago, Chile

**Abstract** Here we show how ultra-high resolution seabed mapping using new technology can help to understand processes that sculpt submarine canyons. Time-lapse seafloor surveys were conducted in the axis of Monterey Canyon, ~50 km from the canyon head (~1,840 m water depth) over an 18-month period. These surveys comprised 5-cm resolution multibeam bathymetry, 1-cm resolution lidar bathymetry, and 2-mm resolution stereophotographic imagery. Bathymetry data reveal centimeter-scale textures that would be undetectable by more traditional survey methods. Upward-looking Acoustic Doppler Current Profilers at the site recorded the flow character of internal tides and the passage of three turbidity currents, while sediment cores collected from the site record flow deposits. Combined with flow and core data, the bathymetry shows how turbidity currents and internal tides modify the seabed. The turbidity currents drape sediment across the site, infilling bedform troughs and smoothing erosional features carved by the internal tides (e.g., rippled scours). Turbidity currents with speeds of 0.9–3.3 m/s failed to cause notable bedform movement, which is surprising given that flows with similar speeds produced rapid bedform migration elsewhere, including the upper Monterey Canyon. The lack of migration may be related to the character of the underlying substrate or indicate that turbidity currents at the site lack dense, near-bed layers. The scale of scours produced by the internal tides ( $\leq 0.7$  m/s) approaches the scale of features recorded in the ancient rock record. Thus, these results illustrate how the scale gap between seabed mapping technology and the rock record may eventually be bridged.

**Plain Language Summary** This study presents the highest resolution repeat seafloor mapping surveys to date in a submarine canyon. Centimeter-scale seafloor surveys were conducted over an 18-month period at a location ~50 km from the head of Monterey Canyon. Turbidity currents (rapid, down-slope density-driven flows of water) and internal tides (tidal currents that flow along the seabed) were recorded by a seafloor instrument node deployed in the study area. Turbidity currents drape sediment across the bedforms, infill troughs, and smooth out erosional features carved by internal tides. While the turbidity currents caused considerable migration of bedforms in the upper canyon, there was surprisingly no notable migration at the study site. The lack of migration may be related to the relatively coarse nature of the seafloor underlying the bedforms and suggests that the turbidity currents at the site lacked a dense near-bed layer characteristic of flows farther up-canyon. The internal tides carved centimeter-scale scours in the seabed, a scale that approaches that of features preserved in the rock record. This study, therefore, shows how new mapping technology may eventually bridge the scale gap between modern seafloor surveys and the ancient rock record.

## 1. Introduction

Seafloor sediment density flows (i.e., turbidity currents) carry globally significant volumes of sediment, nutrients, and organic carbon to the deep sea (Canals et al., 2006; Galy et al., 2007). They are economically significant, as they can break valuable seabed pipelines (Bruschi et al., 2006), and communications cables (Carter et al., 2014), while their deposits may host important oil and gas reserves (Weimer & Link, 1991). Despite this importance, turbidity currents remain understudied due to their unpredictability and the notoriously challenging nature of measuring them in situ in the deep sea. Turbidity currents that move through submarine canyons have been directly measured at only ~10 sites worldwide (Table S1). Even fewer sites (~3) have combined detailed

turbidity current monitoring with both coeval sediment coring and time-lapse mapping. These locations include Squamish Delta in British Columbia (Hage et al., 2018; Hughes Clarke, 2016), Pointe-des-Monts in the Gulf of Saint Lawrence (Normandeau et al., 2020, 2022) and Monterey Canyon (Paull et al., 2018; Symons et al., 2017). These studies were all in relatively shallow water at survey resolutions of 30 cm to >2 m.

In addition to turbidity currents, internal tides (internal waves that oscillate at tidal frequencies) also characterize many submarine canyons (Hall & Carter, 2011). Internal wave and tide deposits are generally thought to be formed by the reworking of turbidity current deposits (Zhenzhong et al., 2013). This is a matter of debate in the literature, however, as the scale of their deposits is too small to be observed with conventional shipborne seafloor mapping in the deep sea and has largely been inferred from the stratigraphic record (e.g., Shanmugam, 2014; Zhenzhong et al., 2013).

The ability to measure morphologic change of the seabed through co-registered, repeated bathymetric surveys is critical to understanding the processes that shape the seafloor. The resolution of surveys largely depends on the distance of the sensors from the seafloor. In the deep ocean, bathymetric surveys from surface vessels using acoustic sensors (e.g., hull-mounted multibeam sonars) achieve resolutions that inversely scale with depth. For example, the vertical resolution for most systems is at best ~0.2%–0.5% of the water depth. Thus, for 2,000-m deep seafloor using a 1° by 1° multibeam sonar, these systems may have a horizontal resolution of ~30 m and a vertical resolution of ~4–10 m. Repeated surveys from ships have been used to detect large-scale changes associated with submarine volcanic eruptions (e.g., Fox et al., 1992), earthquakes (e.g., Fujiwara et al., 2011; Mountjoy et al., 2018), hurricanes (e.g., Miner et al., 2009), and submarine channel evolution (Heijnen et al., 2020). By bringing acoustic sensors closer to the seafloor, remotely operated vehicles (ROVs) and autonomous underwater vehicles (AUVs) successfully map at finer scales, typically about a 1-m horizontal resolution, when surveying at altitudes of 50-m above the seafloor. Examples of seafloor change observations at these scales include seafloor alterations after turbidity flows in a submarine canyon (e.g., Paull et al., 2010, 2018) and after the emplacement of lava flows (e.g., Caress et al., 2012). When surveys are conducted from altitudes less than ~10 m, acoustic sensing can be augmented with optical methods such as photography and laser scanning, and depending on the altitude and sensors, the resolution of the observations can be improved to centimeters or even millimeters (e.g., Roman & Mather, 2010).

Here we present the highest-resolution (cm—mm) repeat surveys collected in the deep (>1 km) sea to date, illustrating how novel technologies can push remote mapping capabilities and further our understanding of how turbidity currents and internal tides modify the seabed. Surveys were conducted using a Low-Altitude Survey System (LASS) developed by the Monterey Bay Aquarium Research Institute (MBARI). The LASS is mounted to an ROV and collects co-located multibeam bathymetry, lidar bathymetry, and stereo color photography, simultaneously mapping the seabed at horizontal resolutions of 5-cm, 1-cm, and 2-mm, respectively. It therefore provides far higher resolution seabed mapping than previously used multibeam echo sounder systems mounted on surface vessel, ROV, or AUV. The spatial resolution of surveys conducted with the LASS approaches that of observations from many rock outcrops (Peakall et al., 2020), showing how the current gap between field studies and the rock record may eventually be bridged.

The LASS was used to conduct four repeat mapping surveys between November 2015 and April 2017 as part of the Coordinated Canyon Experiment (CCE; Paull et al., 2018). The CCE was a multi-institution effort to characterize the nature and impact of turbidity currents within Monterey Canyon, offshore California (Heerema et al., 2020; Maier et al., 2019; Paull et al., 2018). The 18-month-long experiment involved more than 50 seafloor and water column sensors, repeat mapping surveys of the canyon axis at a 1-m scale utilizing AUVs, and sediment sampling via ROV-acquired pushcores and vibracores. The LASS surveys focus on a small (~20,000 m<sup>2</sup>) area of seafloor that is located near the end of the instrument array, ~50 km from the canyon head in water depths of ~1,840 m (Figures 1a and 1b).

A seafloor-resting instrument frame, herein referred to as the Seafloor Instrument Node (SIN), was deployed within the LASS survey area (Figure 1b). The SIN hosted three upward-looking Acoustic Doppler Current Profilers (ADCPs), which continuously monitored current velocities and directions and recorded the passage of three turbidity currents during the CCE. The SIN thus provided unusually detailed direct measurements of flows that caused changes in seabed geomorphology. Six moorings with ADCPs were deployed along the canyon axis from water depths of ~300 to 1,850 m and recorded a total of 15 flows (Figures 1a and 1c). Three fast-moving turbidity currents with front speeds of 2–8 m/s in the upper canyon traveled through the entire mooring array to reach

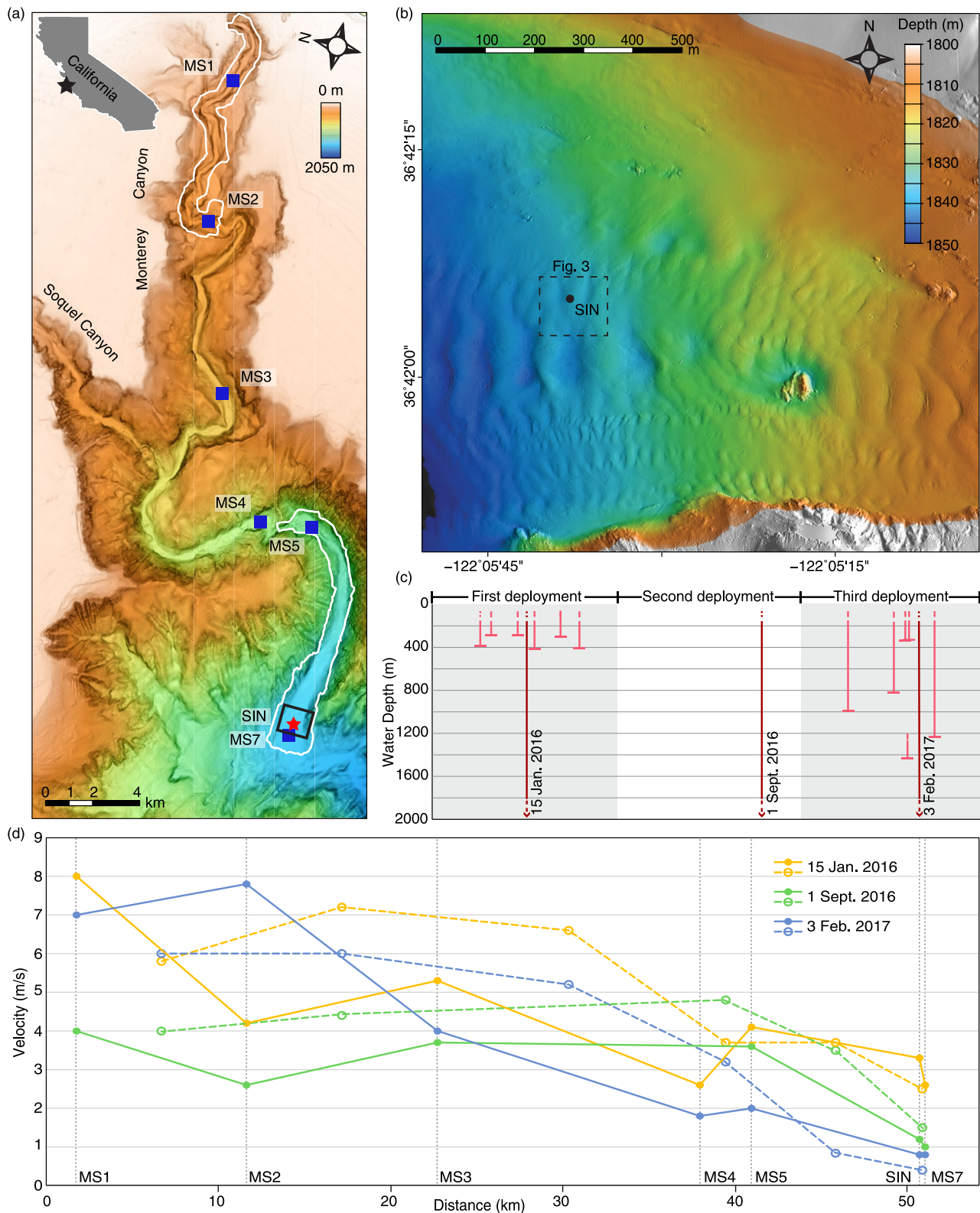


**Figure 1.** Maps of the mooring locations with autonomous underwater vehicle survey locations outlined in white (a) and the location of the study site (b). (c) Occurrence and run-out depth of the 15 turbidity flows that occurred during the Coordinated Canyon Experiment. (d) Flow (solid lines and circles) and transit (dashed lines and open circles) velocities for the three turbidity flows that traversed the whole instrument array, as measured by the acoustic Doppler current profilers on the Seafloor Instrument Node.

the SIN at 1,840 m depth (Figure 1d; Heerema et al., 2020; Paull et al., 2018). The remaining turbidity currents terminated before the SIN, although some of the events were still powerful enough to move very heavy (695 kg in water) objects at speeds  $\geq 4$  m/s for several kilometers (Paull et al., 2018). The movement of these heavy objects was used to infer that these flows contained a dense near-bed layer in the upper canyon (Gwiazda et al., 2022; Heerema et al., 2020; Paull et al., 2018). Together with the tracking of boulder-shaped, motion-sensing devices in the upper canyon (Gwiazda et al., 2022), the ADCP moorings provided insight into the wider evolution and character of turbidity currents that reached the SIN. A series of precisely located vibracores and pushcores was also collected within the LASS survey area. These cores characterize the deposits left behind by sediment flows during the period in which both flow events and seabed geomorphology were monitored, furthering our understanding of how the flow processes are recorded within seabed deposits.

The overall objective of this study is to demonstrate how advances in seafloor mapping can achieve significantly higher resolution surveys and thus advance knowledge of seafloor processes, especially when combined with detailed flow monitoring and precision coring. Our primary goal is to understand the origin of the geomorphic features observed in the detailed seafloor surveys of the study area in Monterey Canyon. Specifically, we seek to understand the origin of the near-linear or convex down-canyon bedforms and why relatively powerful (m/s) turbidity currents fail to cause significant bedform migration. We discuss the wider implications for how such bedforms may record submarine flow processes, and why flows with similar speeds cause rapid migration of crescent-shaped bedforms in the upper parts of Monterey Canyon and at other sites worldwide. We also show how internal tides can modify the seafloor and how they may be recorded by small-scale scours and seabed deposits within Monterey Canyon.

## 2. Background to the Study Site: Monterey Canyon

Monterey Canyon is the most closely studied submarine canyon in the world (De Leo & Puig, 2018) and is the largest canyon along the western coast of the United States. The canyon contains a submarine channel system that extends over 400 km seaward to a depth of more than 4,000 m on the abyssal plain (Paull et al., 2011). The floor of the canyon is underlain by sand and coarser-grained sediment that is mainly deposited by turbidity currents taking place on a sub-annual recurrence (e.g., Bailey et al., 2021; Heerema et al., 2020; Maier et al., 2019; Paull et al., 2010, 2018; Xu et al., 2004). Previous work indicates that turbidity currents in the upper canyon likely contain fast and dense near-bed layers, generated by the remobilization of the seabed (Gwiazda et al., 2022; Heerema et al., 2020; Paull et al., 2018).

Bottom currents within Monterey Canyon are driven by a semidiurnal internal tide (Hall & Carter, 2011). Internal tides are formed when surface tides move stratified water up and down the sloped terrain within the axes of submarine canyons (Pomar et al., 2012). Mean bottom current magnitude varies significantly throughout Monterey Canyon, from commonly  $>50$  cm/s in the narrow uppermost canyon to  $\sim 5$  cm/s out on the deep-sea fan. At our study site, internal tide velocities reached 70 cm/s. The topography of the canyon traps open-ocean internal waves, known to generate strong bottom currents, enhance turbulence, and produce internal tidal bores as they propagate up canyon (Key, 1999; Kunze et al., 2002; Petrucio et al., 1998; Xu & Noble, 2009). Previous work has proposed models for how internal tides modify the seafloor via erosion and deposition, and how internal tides are recorded in deposits and the rock record (Pomar et al., 2012). However, these previous models are poorly tested against modern field data, especially those combining detailed time-lapse mapping with both flow monitoring and cores.

Crescent-shaped bedforms, with crests that are convex in an up-canyon direction, are nearly ubiquitous along the floor of upper Monterey Canyon, extending out to water depths of at least 2,100 m (Figure 1a; Paull et al., 2011; Smith et al., 2005; Xu et al., 2008). The origin of these bedforms has been linked to instabilities (cyclic steps) in supercritical (fast and thin) turbidity currents (e.g., Hughes Clarke, 2016), which also have a dense layer at their base (Paull et al., 2018). These active bedforms have wavelengths of 50–80 m and amplitudes of up to 2.5 m. Recent studies show how fast-moving turbidity currents with front velocities of  $\sim 4$ –7 m/s may cause rapid upslope migration of crescent-shaped bedforms (Paull et al., 2010). Repeat AUV surveys every  $\sim 4$  months during the CCE show that these bedforms migrate several meters up-canyon and produce widespread bathymetric changes of  $\pm 3$  m (Paull et al., 2018). Our study site lies within a train of large bedforms that have a different morphology, with crests that are convex down-canyon or more linear. These reverse curvature bedforms are up to 10 m in amplitude and have wavelengths that are significantly longer (150–200 m) than those of the crescentic

bedforms seen farther up the canyon (Paull et al., 2011). Interwoven with these reverse-curvature bedforms, along their northern termination within the study area (Figure 1a), is a set of much more linear-crested bedforms with amplitudes up to 2 m and wavelengths of 50–80 m. It is on the crest of one of these smaller, more linear bedforms that the SIN was deployed, and the LASS surveys were centered.

### 3. Methods

#### 3.1. LASS System Data Collection and Processing

Centimeter-scale bathymetric surveys were conducted with the LASS, a prototype 1-cm resolution low-altitude seafloor mapping system. The survey system included a Reson SeaBat 7125 400-kHz multibeam sonar, a 3D at Depth SL1 subsea lidar, two Prosilica 2.8 MPixel color stereo cameras, two Ocean Imaging Systems 3831 strobe lights, a Paroscientific Digiquartz 8CB4000 pressure sensor, and a Kearfott SeaDevil inertial navigation system (INS) aided by a 300-kHz RDI Workhorse Doppler Velocity Log (DVL). The ROV survey lines were flown at a speed of 0.2 m/s (~0.4 knots) and LASS altitude of 2.5 m, using a 1.2-m line spacing to ensure 100% lidar coverage. Survey lines were run automatically using ROV control software operating with real-time INS navigation and DVL altitude. This multibeam sonar produces a 140° swath composed of 512 beams with an along-track (transmit) and across-track (receive) beamwidth of 1° and 0.5°, respectively, corresponding to a nadir beam footprint of 4 by 2 cm. Only the inner 120° (~8.5 m) of soundings were used due to increased noise in the outer beams. The SL1 lidar system pulses a laser at a rate of 40 kHz, directed through scanning mirrors to cover a 30° wide field of view (~1.3 m at 2.5-m altitude) with 240 pulses per across-track scan. The nadir beam footprint of the lidar is ~1.75 mm. Lidar beam spacing is greatest at nadir (~1 cm) and less toward the edges of the swath as the scanning mirror slows down to change directions. The stereo color images were taken at 0.5 Hz (or every 0.4 m along track) and have an across-track extent of 4.1 m, an along-track extent of 3.1 m, and a pixel size of ~2 mm. Each of the four repeat surveys of the study is composed of multiple ROV dives, during which the LASS mapped ~850 m<sup>2</sup> per hour with the lidar system.

The INS integrates three orthogonal accelerometers with a ring laser gyroscope to measure angular velocity and linear acceleration, providing position and orientation of the ROV relative to a previous position. The DVL uses four acoustic beams to estimate velocity relative to the seabed. Assuming that the DVL maintains a continuous bottom lock on the seabed, the real-time navigational drift is less than 0.05% of the total distance traveled. The pressure sensor was used to measure vehicle depth with a precision of ±2 cm and an absolute depth accuracy of 20 cm. The INS was initialized prior to deployment using a GPS receiver. During ROV descent, ultra-short base-line (USBL) tracking was used to stabilize the INS fix. Once the DVL achieved bottom lock at ~30 m altitude, the USBL aiding was ended.

MB-System (v. 5.7.6), an open-source software package for the processing and visualization of bathymetry and backscatter data (Caress & Chayes, 1996; Caress et al., 2020), was used to process the multibeam sonar and lidar bathymetry data. For each survey, offsets in LASS navigation were corrected using MBnavadjust, a tool within MB-System that measures relative navigational offsets in overlapping and crossing swaths by matching bathymetric features, and then solves for an optimal, self-consistent navigation model. The multibeam bathymetry, which has more than 200% overlap, was used for the navigation adjustment. Multiple passes conducted over the SIN (Figure 2) during each survey allowed it to be used as a primary feature in the individual navigation correction. Other features used in the correction for each individual survey include boulders, depressions, and matching patterns of deepening or shallowing contours. The relative lateral precision of the adjusted navigation model is equivalent to the 5-cm lateral resolution of the bathymetry data. The navigation model obtained from the multibeam bathymetry was also used to correct the navigation for the coincident lidar data and stereo imagery.

After navigation models were computed and applied to the four individual surveys to make them internally consistent, MBnavadjust was used to co-locate the repeat surveys in relation to each other. A prominent large boulder identified in all four surveys (not visible in Figure 3, but clearly visible in Figure 4) was used to tie the surveys together, with the *X*, *Y*, *Z* offset estimated through cross-correlation. The assumption that the absolute position of the boulder did not change between surveys is supported by the observation that the distinctive pattern defined by the position of the boulder relative to other nearby boulders did not change. The SIN was used as an additional tie point in the co-location of the final two surveys as it was not recovered during the interim period and there is no evidence from the attitude sensors within the ADCPs to suggest it moved during that time. The

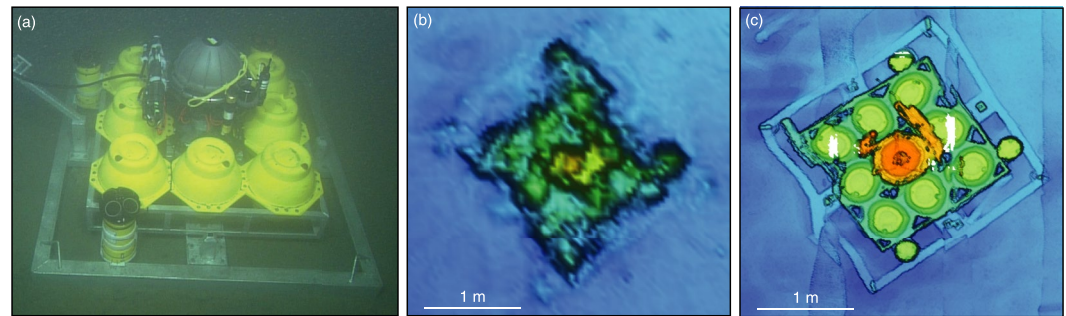


**Figure 2.** The Seafloor Instrument Node (SIN). The SIN's square iron frame is 2.2 m long on a side. (a) Video frame-grab from the remotely operated vehicle collected after the first deployment. (b) 5-cm resolution multibeam bathymetry over the SIN. (c) 1-cm resolution lidar bathymetry over the SIN. Distortions of the SIN seen in panel (c) are related to mismatches in the centimeter scale navigation corrections.

relative vertical precision between the surveys, estimated by the misfit in the final grids at the boulder tie point, is found to be no more than 2 cm.

Once the bathymetric data were processed and the navigation correction applied, the data were gridded at a lateral resolution of 5 cm for the multibeam sonar bathymetry and 1 cm for the lidar bathymetry. The same latitude and longitude bounds were used for each bathymetric grid, which when combined with the same lateral resolution, ensured that the grid cells in each of the 4 repeat surveys were co-registered, allowing for difference grids to be generated by subtracting one grid from another.

### 3.2. Flow Monitoring

A remarkably detailed array of sensors documented turbidity currents and internal tides during the 18-month CCE experiment. This sensor array measured velocities and other key characteristics of flows that caused the changes in seabed morphology documented by time-lapse bathymetric surveys. The full array of sensors is described in more detail by Paull et al. (2018), but it included a series of 6 moorings, each of which housed a 300 kHz ADCP that pointed downward at the seabed, typically from an elevation of 65 m. These ADCP-moorings (MS1–MS7 in Figure 1a) were located from water depths of ~300 m (MS1) to ~1,850 m (MS7). They recorded arrival times of turbidity currents, from which front speeds between moorings were calculated, and provided time series of velocities for both turbidity currents and internal tides.

The 45 kg (in water) SIN was deployed in ~1,840 m water depth (Figures 1a and 2) and hosted three upward-looking Teledyne/RDI Workhorse Sentinel ADCPs, with operational frequencies of 300, 600, and 1,200 kHz. The ADCPs were mounted such that the transducer heads were ~0.5 m above the seabed. For the purpose of this study, we only show data from the 600 and 1,200 kHz ADCPs, as the 300 kHz stopped working during the second deployment and did not capture all three events that reached the study site. The 600 kHz ADCP measures flow in 0.5-m intervals (bins) from 2.1–38.6 m above the bed and shows the full thickness of the flows. The 1,200 kHz ADCP records data in 0.25-m intervals, from 1.31–11.31 m above the bed, providing the best vertical resolution of the flow structure closest to the seabed.

### 3.3. Vibracores and Pushcores

In April 2017, approximately 2 weeks after the final CCE instrument recoveries, seven vibracores up to 86 cm in length were collected via ROV within the study area. A total of 41 ROV-collected pushcores up to 23 cm long were collected close to seven of the vibracore sites. An additional 16 pushcores were taken at two scour locations, four cores collected inside each scour and four cores collected just outside. Vibracores were split and scanned with a Geotek digital line-scanning camera. For each group of pushcores from a single location, one to two were extruded, photographed, and described.

## 4. Results

We first summarize results from time-lapse surveys in the main study area at ~1,840 m water depth. This is followed by a summary of flow monitoring data from the SIN and sediment cores from that same area.

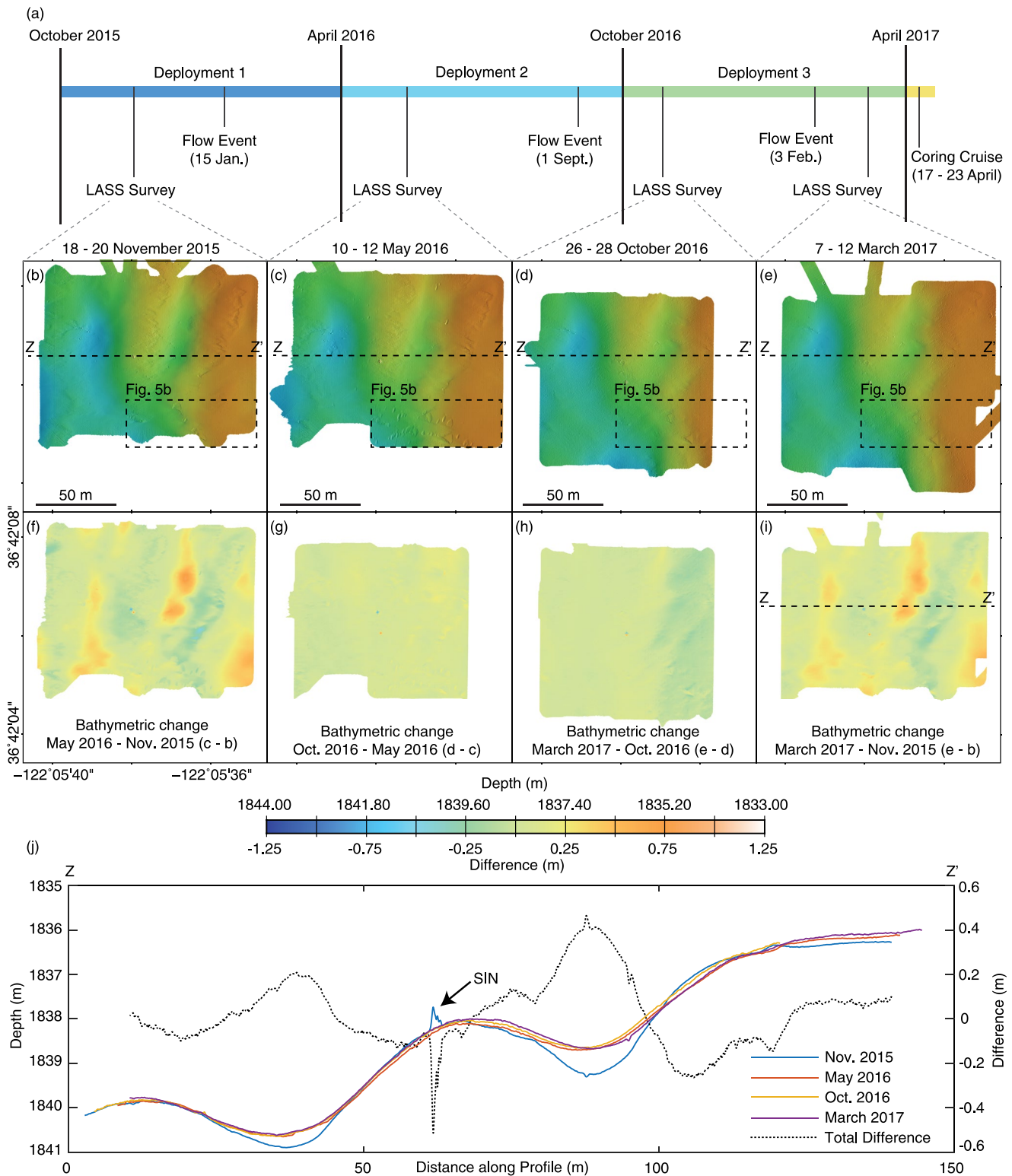


**Figure 3.** Repeat mapping shows bathymetric change over the course of the Coordinated Canyon Experiment (CCE). (a) Timeline of the CCE experiment, surveys, and turbidity currents. (b–e) Color-shaded sonar bathymetry from the four Low-Altitude Survey System surveys gridded at 5 cm. (f–i) Bathymetric difference grids. Panels (b)–(i) share the same spatial extent, as shown in panel (f). (j) Profiles and cumulative bathymetric difference (March 2017–November 2015) along Z–Z'.

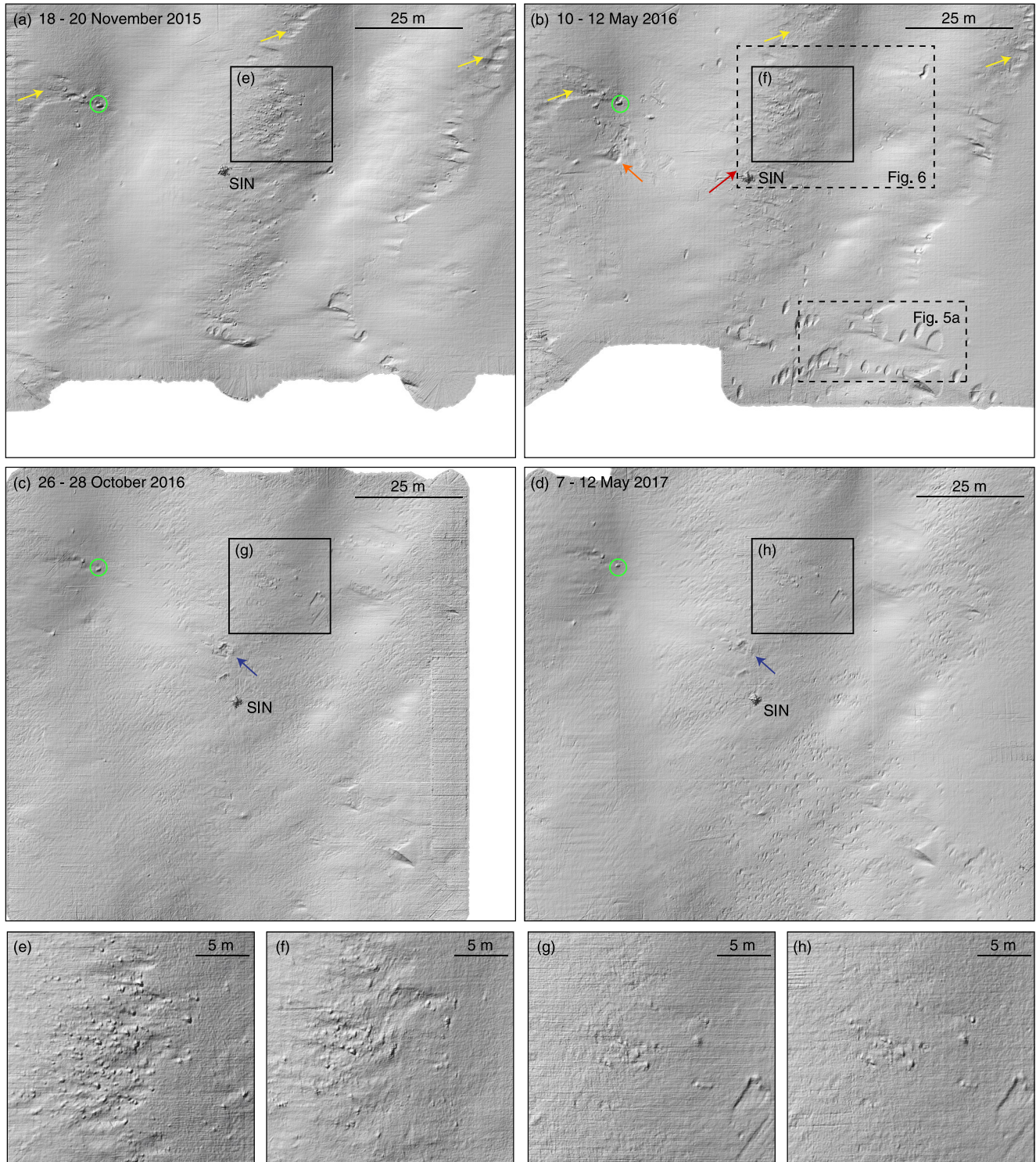


**Figure 4.** Grayscale bathymetry highlights textures and small-scale features. (a–d) Sonar bathymetry from the four repeat Low-Altitude Survey System mapping surveys gridded at a resolution of 5 cm. Green Circle: meter-scale boulder used to co-locate the four surveys. Yellow arrows: fluted erosional texture visible on the crests of the bedforms. Red arrow: deployed location of the Seafloor Instrument Node (SIN) in October 2015. Orange arrow: scour pit left by the SIN after it was recovered in April 2016. Dark blue arrow: depression that formed around the SIN during the second 6-month-long deployment. The black solid square outlines a boulder field north of the SIN and is shown in panels (e–h).

#### 4.1. Time-Lapse Bathymetric Surveys

The LASS survey area shallows west to east from 1842 to 1834 mwd (Figure 3). Color-coded bathymetry (Figures 3b–3e) is used to show the general surface morphology of the study area, while grayscale bathymetry is used to highlight seabed textures and small-scale features (Figure 4). Changes in the morphology of the seabed associated with the passage of turbidity and ambient tidal currents are highlighted by difference maps, made by subtracting the previous survey from the subsequent one (Figures 3f–3i). The SIN was deployed on the crest of the central bedform during each of the deployments, and it is clearly visible in both the multibeam and lidar bathymetry for all four surveys (Figures 3 and 4). A timeline of the surveys in relation to the turbidity currents is given in Figure 3a.

##### 4.1.1. Initial Survey: 18–20 November 2015

The first LASS survey of the study site was conducted approximately 1 month after the first deployment of the SIN. The most prominent features are the three bedforms and two intervening troughs, with a wavelength of ~50 m and amplitude of ~2 m (Figure 3b). Patches of partially buried boulders, with visible tops up to ~0.5 m across, are imaged on the crest of the central bedform both north and south of the SIN. Larger isolated boulders, with tops >1 m in diameter, occur in the troughs and on the flanks of the bedforms, including the one used to co-locate the surveys (green circle, Figure 4a). The seafloor in the southern portion of the survey area is relatively smooth, except for a couple of meter-scale scours and a larger crescent-shaped pit. A fluted erosional texture marks the crests of all three bedforms (yellow arrow, Figure 4a).

##### 4.1.2. Second Survey: 10–12 May 2016

The second LASS survey (Figures 3c and 3f) reveals considerable bathymetric change since the initial survey. Substantial deposition of sediment in two distinct areas occurred in the trough between the central and eastern bedforms. The southern area shows a net deposition of ~60 cm, while the northern area shows a net deposition of up to ~80 cm. Net erosion of up to ~40 cm occurred along the lee side of the eastern bedform (Figure 3j).

In April 2016, during the ROV dive to recover the SIN for scheduled servicing, it was discovered that the SIN had moved ~26 m down canyon from its deployed position (red arrow, Figure 4b). The SIN was found partially buried in a few centimeters of sediment; a scour pit is visible at the recovery location (orange arrow, Figure 4b).

Fewer boulders are visible within the boulder fields near the SIN, as the stoss side of the bedform crests were draped with 5–10 cm of sediment (Figure 4f). Scouring is observed around some of the boulders still visible in the southern boulder field. The fluted erosional features on the crest of the bedforms are less apparent, particularly along the central bedform (yellow arrows, Figure 4b). The crescent-shaped pit near the eastern bedform observed in the first survey is no longer visible.

In the southeastern portion of the survey area, where a few scours were previously visible, a field of meter-scale scours has developed (Figures 4b and 5). Individual scours are up to 2 m in width, 4 m in length, and 20 cm in depth. A second, smaller set of scours (~0.5 m wide, 2 m long, 8 cm deep) extends northwest. All scours have an average orientation of  $19^\circ (\pm 5^\circ)$  from north. Up to ~1.9 m<sup>3</sup> of material is estimated to be excavated from individual scours. The edges and bottoms of the scours, as well as the surrounding seafloor, appear smooth in the 5-cm resolution multibeam bathymetry. The 1-cm resolution lidar bathymetry, however, reveals that the scours have a centimeter-scale internal ribbing and the seafloor extending from the northern end of some of the larger scours is mottled (Figure 5a). The internal ribbing has wavelengths of 3–17 cm and amplitudes of 2–4 cm, with downstream-oriented arcuate crests and troughs that extend longitudinally across the scours. The mottled texture has wavelengths varying between 6 and 9 cm and amplitudes between 1 and 2 cm (Figure 5c). The seafloor around the sides and southern end of the scours is relatively smooth. The photomosaics show that some of the scours contain sediment that is significantly darker than that of the ambient seafloor, which may be indicative of finer-grained mud (Figure 5f). There are also color variations that appear to form ripple-like bands on the seafloor between the scours, which are not discernible in either the multibeam or lidar bathymetry that may indicate the presence of micro-ripples.

A series of west-northwest trending lineations within the boulder field just northeast of the SIN is discernible in both the multibeam and lidar data sets (Figures 4e, 6a, and 6b). These lineations are 2.5–3.5 m in length and 10–15 cm in height and primarily fall within the area that experienced little to no erosion ( $\leq 1$  cm). In the trough between the central and eastern bedforms, the northern depositional area is marked by hundreds of small pits only discernible

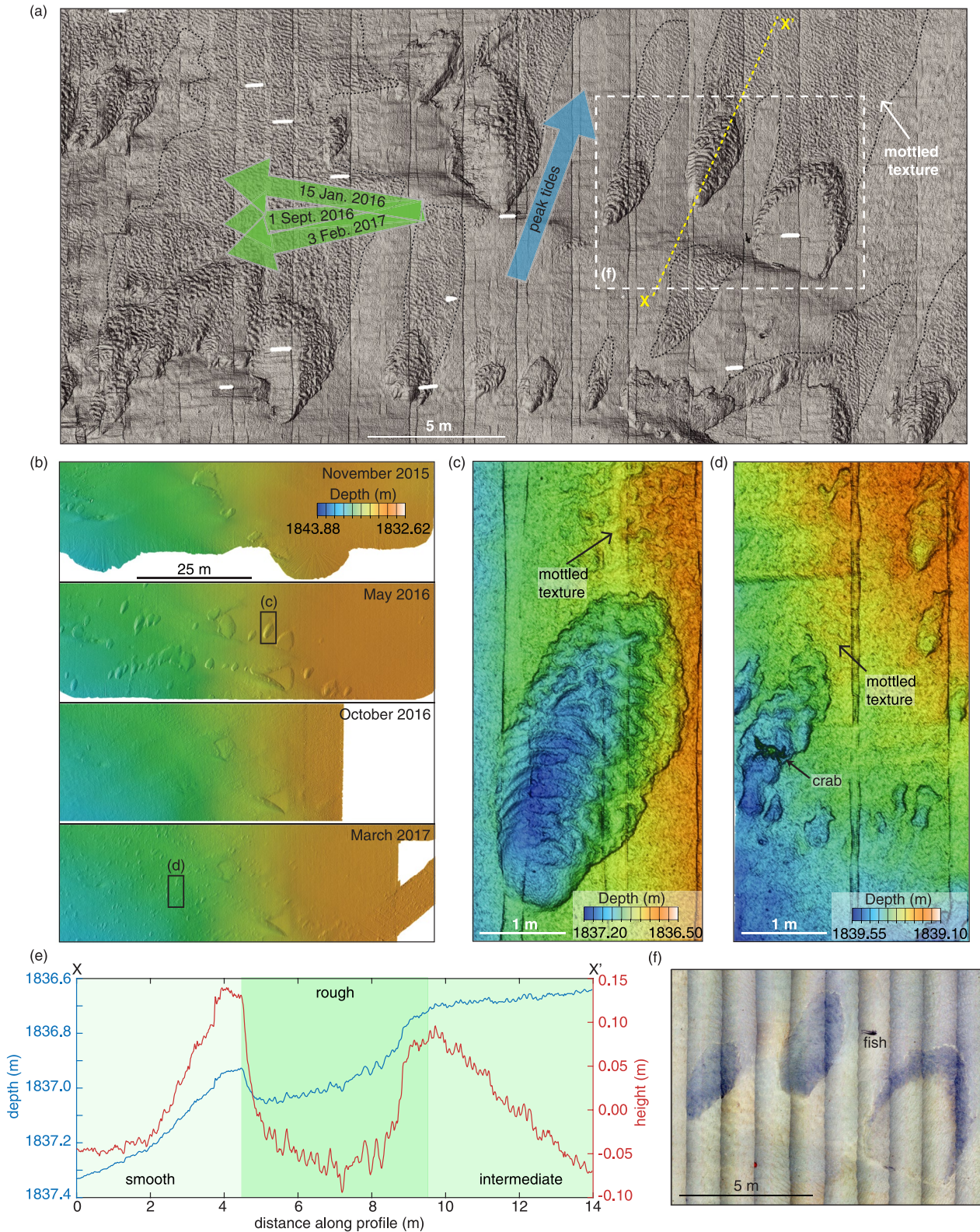


**Figure 5.** Scour fields. (a) Lidar bathymetry of the scour field obtained in the May 2016 Low-Altitude Survey System survey, gridded at 1-cm resolution with a 3X vertical exaggeration to highlight the textures. Green arrows show the flow direction of the three turbidity currents as measured by the Seafloor Instrument Node. Blue arrow denotes the direction of the peak spring internal tides. (b) 5-cm sonar bathymetry of the scour area for all four surveys as denoted in Figure 3. (c) and (d) 1-cm lidar bathymetry showing detailed structure of the scours called out in panel (b). (e) Profile X—X' as denoted in panel (a), showing both depth and detrended height across one of the scours. (f) 2-mm resolution photomosaic of the area denoted by the dashed white box in panel (a).

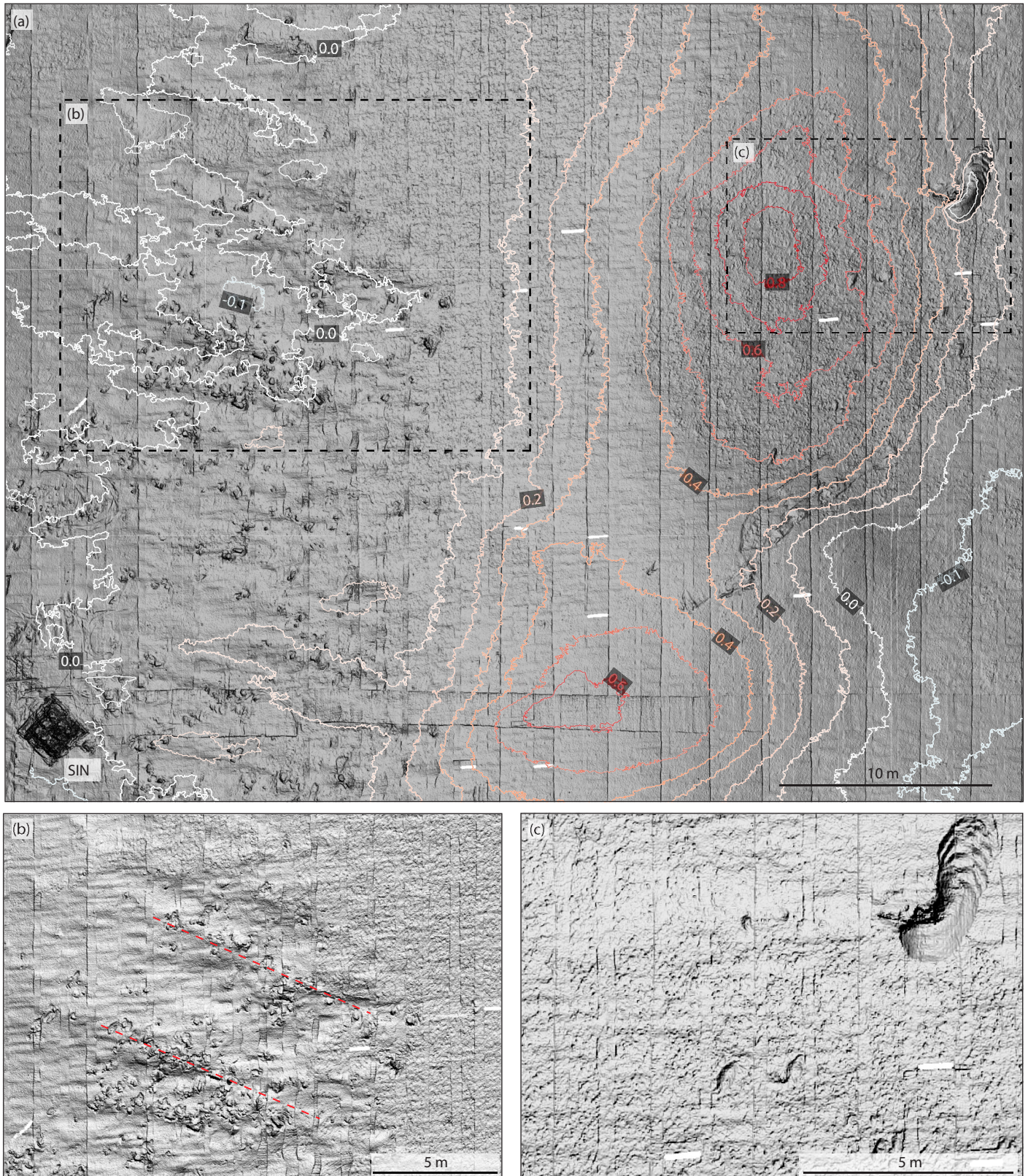


Figure 6.

in the lidar data (Figure 6c), while the southern depositional area is relatively smooth. The pits are 3–4 cm wide and 1–2 cm deep. The transition from the pitted texture to the adjacent smooth seafloor is rather sharp (Figure 6c).

#### 4.1.3. Third Survey: 26–28 October 2016

Between the second and third surveys, a sediment drape, at least 5–10 cm thick, was deposited throughout most of the survey area, with net deposition reaching up to 20 cm in the northeastern corner along the crest of the eastern bedform (Figures 3d and 3g). The most substantial change is in the southeastern quadrant of the survey area where the meter-scale scours have been smoothed out (Figures 3d, 4c, and 5b). The field of boulders south of the SIN appears to be entirely buried, while the tops of some of the larger boulders north of the SIN are still visible (Figures 4c and 4g). The fluted erosional features along the crests of the bedforms seem to be almost entirely smoothed out. The meter-scale scours at the southern edge of the central bedform are gone, with only a couple of smaller scours and the top of the small topographic high visible (Figure 4c). Minimal erosion, on the order of only 1–2 cm, is indicated on the lee side flank of the bedforms (Figure 3g).

#### 4.1.4. Final Survey: 7–12 March 2017

The final LASS survey of the CCE documents the morphologic change since the previous survey, as well as the net change over the CCE. Between October 2016 and May 2017, a 5-cm sediment drape was laid over much of the survey area. Up to 18 cm of net deposition occurred in the trough between the central and eastern bedform (Figures 3e and 3h). Along the lee side and crest of the eastern bedform, at least 10–30 cm of sediment has been eroded (Figure 3h).

Several sub-meter scale scours are visible in the southcentral and eastern portion of the survey area, including the region that was previously populated by meter-scale scours in the May 2016 survey (Figures 4d and 5b). The number of scours in this region totals in the hundreds and the extent of the scour field extends farther north than the meter-scale scour field observed in May 2016. The orientation of these scours is more varied than the May 2016 scours, though the average orientation,  $21^\circ \pm 6^\circ$  from north, is still in agreement. The average depth within the scours is ~5–10 cm. Similar to the larger May 2016 scours, these scours appear smooth in the 5-cm multibeam bathymetry, while in the 1-cm lidar bathymetry, some scours show the same cm-scale internal ribbing (Figure 5d). A mottled texture is also visible extending from the northeastern tip of some of the scours; however, the wavelength and amplitude associated with this texture (~3 cm and <1 cm, respectively) are smaller than those observed in the May 2016 survey.

The cumulative change between the final and first surveys shows a pattern of deposition in the troughs of the bedforms with erosion predominantly concentrated on the lee side of the eastern bedform (Figures 3i and 3j). The most significant changes over the course of the CCE are those that occurred between the first and second surveys, where at least 80 cm of sediment was deposited in the trough between the central and eastern bedform, and at least 40 cm of sediment was eroded along the lee side of the eastern bedform. The stoss side of the bedforms is being successively built up, with each consecutive survey showing a layer of deposition (Figure 3i).

## 4.2. Flow Monitoring

### 4.2.1. Turbidity Currents

Three relatively powerful turbidity currents ran out for ~50 km through Monterey Canyon to reach the SIN during the CCE experiment (Figure 1c). These turbidity currents had front speeds of 4–6 m/s in the upper canyon but decelerated to front speeds of 0.8–3.7 m/s by the time they passed the SIN (Figure 1d). This deceleration may have been driven by significant widening of the canyon floor upstream from the SIN (Figure 1; Heerema et al., 2020; Paull et al., 2018).

**Figure 6.** 1-cm resolution lidar bathymetry from the May 2016 Low-Altitude Survey System survey. (a) A portion of the survey area showing the areas of max deposition and the lineations along the crest of the central bedform (for location, see Figure 4b). Contours denote the net amount of deposition or erosion that occurred between the November 2015 and May 2016 surveys and are derived from the sonar bathymetry. Contours range from –0.1 to 0.8 m in 0.1-m intervals. The contours around the Seafloor Instrument Node, or with a total length <5 m, were removed for clarity. Vertical exaggeration: 2X. (b) Zoomed in view of some of the northwest-southeast trending lineations as denoted in panel (a). Red dashed lines highlight two of the lineations. (c) Zoomed in view of the pits as denoted in panel (a). Vertical exaggeration in panels (b) and (c) is 3X.

The three ADCPs mounted on the SIN recorded current magnitudes and directions within the LASS survey area throughout each of the three 6-month-long deployments. The arrival of the turbidity currents at the SIN (15 January 2016, 1 September 2016, and 3 February 2017) was marked by a sudden increase in current velocity and acoustic backscatter, as measured by the ADCPs, with flow direction oriented down-canyon (245°–295°, Figures 5a and 7). Of the three flow events, the 15 January 2016 event was the strongest, having a maximum internal velocity (highest ADCP-measured velocity) of 3.3 m/s at the SIN (Figure 7a). The 1 September 2016 event had a maximum internal velocity of 1.2 m/s at the SIN (Figures 7a and 7c). The 3 February 2017 event was the weakest of the three with a maximum internal velocity of 0.9 m/s at the SIN (Figure 7a).

Compasses and attitude sensors in the ADCPs indicate that the SIN moved during 15 January 2016 event but did not move during the subsequent two events. The SIN moved ~26 m down the canyon and came to rest in the trough between the western and central bedforms (orange arrow; Figure 4b). ADCPs on the SIN continued to record data after the SIN moved. The orientation of the ambient currents in this area was rotated by ~25° from the orientation observed at the original deployed location of the SIN. The exact difference in orientation was not the same across all three ADCPs, suggesting that the ADCPs may have rotated within the frame of the SIN or lost their calibrations. As such, data from SIN between the 15 January 2016 event and the recovery in April 2016 were considered suspect and were not used for further analysis.

#### 4.2.2. Internal Tides

The ambient tidal currents recorded at the SIN, excluding the event intervals, show a semidiurnal frequency with a mean current velocity of ~0.2 m/s (Figure 7b). Peak up-canyon tidal velocities were oriented between 350 and 40° and reached 0.6 m/s near the seafloor, while farther up in the water column (8–11 m above the bed) velocities exceeded 0.7 m/s. Peak down-canyon tidal velocities were oriented between 235 and 260° and reached between 0.3 and 0.4 m/s near the seafloor and >0.5 m/s 8–11 m above the seabed (Figure 7d). Peak tidal velocities were associated with spring tides, occurring approximately every 15 days, within 2 to 3 days of a new or full moon (Figure 7b).

### 4.3. Sediment Cores

#### 4.3.1. Vibracores

In April 2017, seven vibracores were collected from the flanks, crest, and adjacent troughs of the central bedform, with recovered lengths ranging from 32 to 86 cm (Figure 8). The cores show fining-upward sequences, starting with base layers of gravels and pebbles overlain by medium- to fine-grained sand with concentrations of dark, organic material. The finer-grained deposits at the top of the cores are thinner in cores recovered from the bedform crest versus the troughs. Plant debris is common near the tops of the cores in or near the troughs. The two vibracores taken from the western trough, 552 and 554, are capped by an ~4-cm thick mud layer. Cores 554 and 555, taken from the western flank of the bedform, show a repeating pattern of fining-upward deposits. Core 556, taken from the crest of the central bedform, has one of the shortest recoveries (34 cm) with ~10 cm of medium-grained sand overlaying gravels and pebbles. Core 548 was sampled from the eastern trough of the central bedform, just south of the area that experienced the greatest amount of deposition during the CCE.

#### 4.3.2. Pushcores

At seven of the vibracore locations, pushcores up to 23 cm long were also taken. Similar to the vibracores, the pushcores show fining-upward sequences of fine to very-fine sand overlain by mud. Most of the cores include plant material mixed in with the sand, while a few bottom out in pebbles and gravel. Some of the pushcores taken within the troughs of the central bedform are capped by 1–2 cm of mud.

Pushcores also sampled two of the sub-meter scours visible in the final March 2017 survey, with one set of 4 pushcores taken inside each of the scours, and one set of 4 taken just outside the scours (Figure 9). The pushcores show sequences of homogeneous fine-grained sand capped by 0.25–2-cm-thick mud, both within and outside the scours. One notable exception is pushcore 49, taken from inside a scour, which is predominantly composed of gravel in a sandy matrix and has no mud cap (Figures 9b and 9d). Three of the cores, two from outside the scour (cores 55 and 57) and one from inside the scour (core 69), contain repeating sequences of mud-capped fining-upward sand (Figures 9d and 9e).

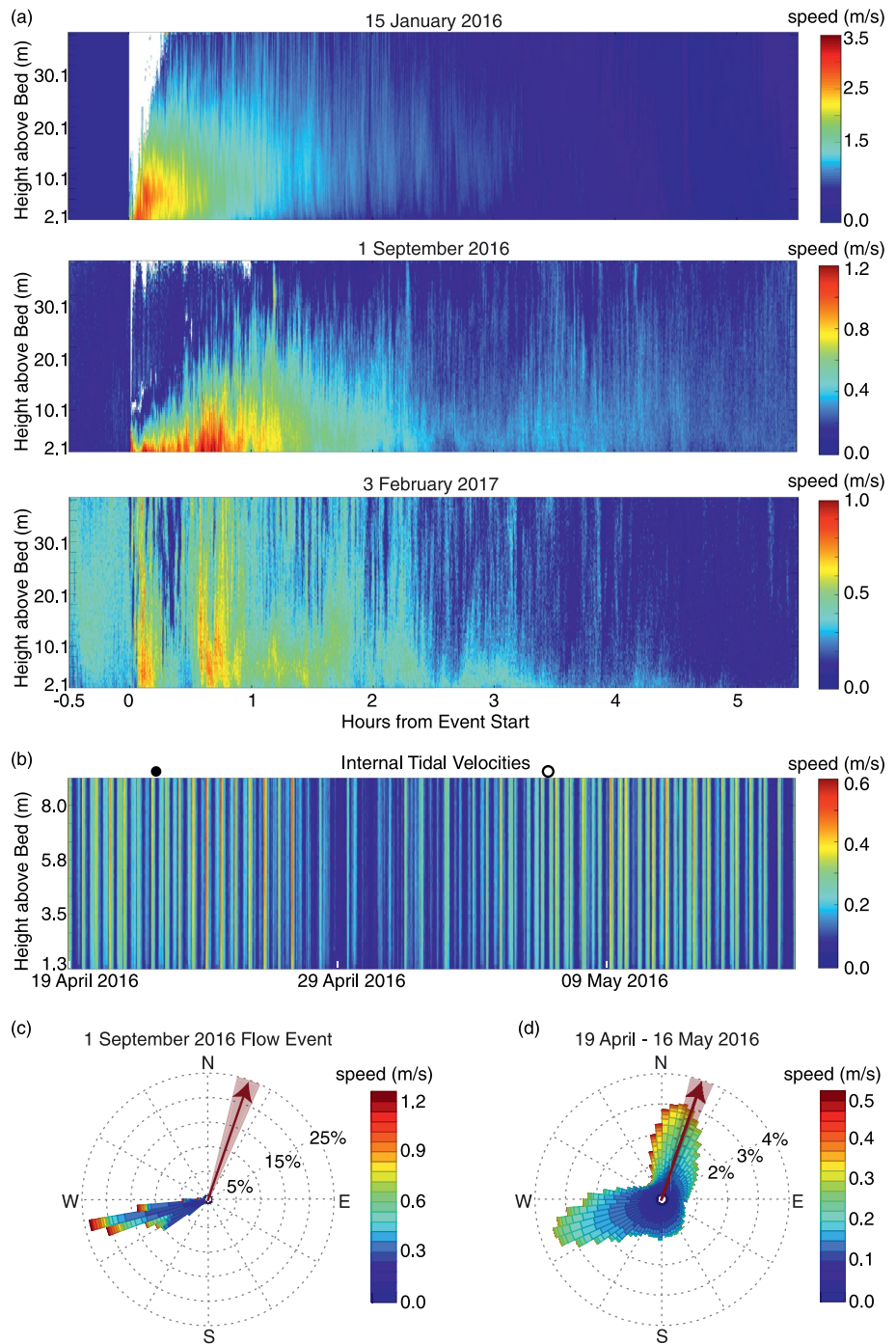


**Figure 7.** Current velocities. (a) Acoustic Doppler current profiler (ADCP)-measured velocities of the three turbidity flows as recorded by the 600 kHz ADCP. (b) One month of internal tidal velocities as measured by the 1,200 kHz ADCP. The timing of the full and new moons is denoted by the solid and open circles, respectively. (c) Rose diagram showing the speeds and direction of the 1 September 2016 turbidity flow. (d) Rose diagram showing the speed and direction of the internal tides over approximately 1 month. The red arrow and associated wedge show the scour orientation of  $19^{\circ} (\pm 5)$ . The currents are binned in  $5^{\circ}$  increments. Timing of the data shown in panels (b) and (d) overlaps the timing of the May 2016 survey when the meter-scale scour field was observed.

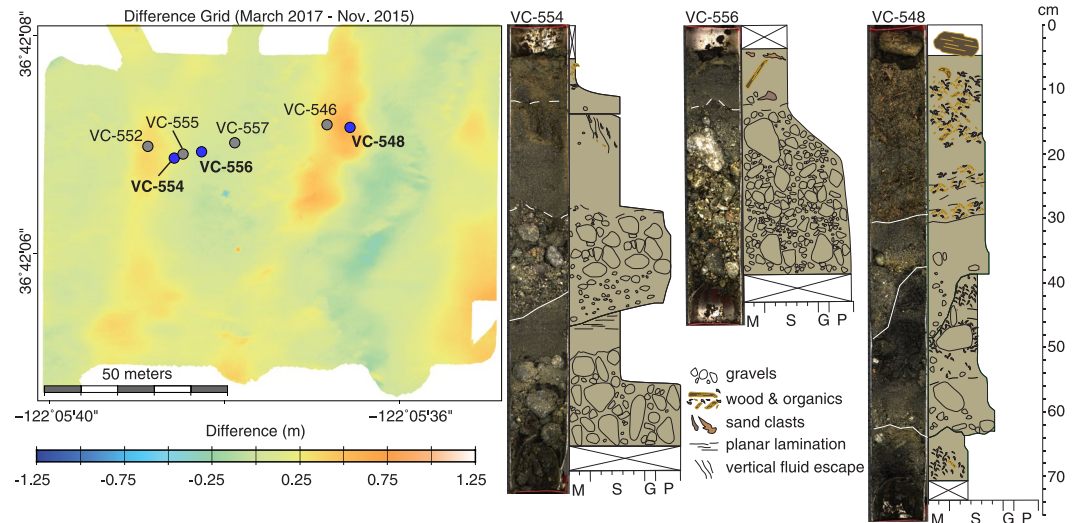


**Figure 8.** Location map and core descriptions for three representative vibracores collected in the study area. The cores are ordered from west to east (down- to up-canyon). The map shows net deposition and erosion between the November 2015 and March 2017 bathymetric surveys. Core locations are shown by circles; blue circles denote the representative cores shown in the figure. White solid lines in core photos mark clear erosional unconformities. Dashed white lines mark inferred erosional contacts.

## 5. Discussion

### 5.1. Origin of Geomorphic Features

#### 5.1.1. Bedform Evolution Due To Turbidity Currents

The repeat seafloor mapping surveys quantify morphologic changes associated with the passage of three turbidity currents during the CCE (Figure 3) and document the smaller-scale effects of tidally driven bottom currents. The front speeds measured in all three turbidity flows were significantly faster at sites farther up canyon (4.8–7.2 m/s; Heerema et al., 2020; Paull et al., 2018), suggesting that these flows had slowed markedly before reaching the SIN. All three flows reworked the seabed and deposited sediment, effectively smoothing out the seafloor. 1 September 2016 and 3 February 2017 flows generally deposited or eroded thin ( $\leq 10$  cm) veneers of sediment (Figures 3g and 3h). These less powerful turbidity currents (internal velocities  $\leq 1.2$  m/s and  $\leq 0.9$  m/s, respectively) produced little change in bedform shape and position. The more powerful 15 January 2016 event resulted in somewhat greater morphologic change, depositing at least  $\sim 80$  cm of sediment in the eastern trough of the central bedform and eroding up to  $\sim 40$  cm off the lee slope of the eastern bedform (Figure 10). If the infilling of the troughs were to continue through multiple flows, the bedforms would subsequently become more poorly developed. This observation suggests that these bedforms may be primarily carved by faster flows than the one seen during the 18-month long CCE (e.g., Mountjoy et al., 2018).

Lineations in the sediment on the crest of the central bedform observed in the lidar bathymetry acquired during the May 2016 survey (Figure 6b) trend west-northwest, following the flow direction of the 15 January 2016 turbidity current. Similar linear grooves have been associated with dense, laminar (debris) flows in other locations (Peakall et al., 2020).

Boulders with tops up to 0.5 m across are aligned along lineations on the crests of the bedforms, which suggests they may also be linked to deposition and/or erosion associated with more powerful, but less frequent, flows.

#### 5.1.2. Scour Field Due To Internal Tides

The meter-scale scour field was surveyed in May 2016, approximately 4 months after the 15 January 2016 event, while the sub-meter scour field was surveyed in March 2017, just 1 month after the 3 February 2017 event (Figures 3c and 3e). The roughly northeastern orientations of both the meter- and sub-meter-scale scours are oblique to the direction of down-canyon flow of the turbidity currents but well-aligned with the incoming internal tidal currents (Figures 5a and 7d), suggesting that the internal tides are responsible for their formation. We

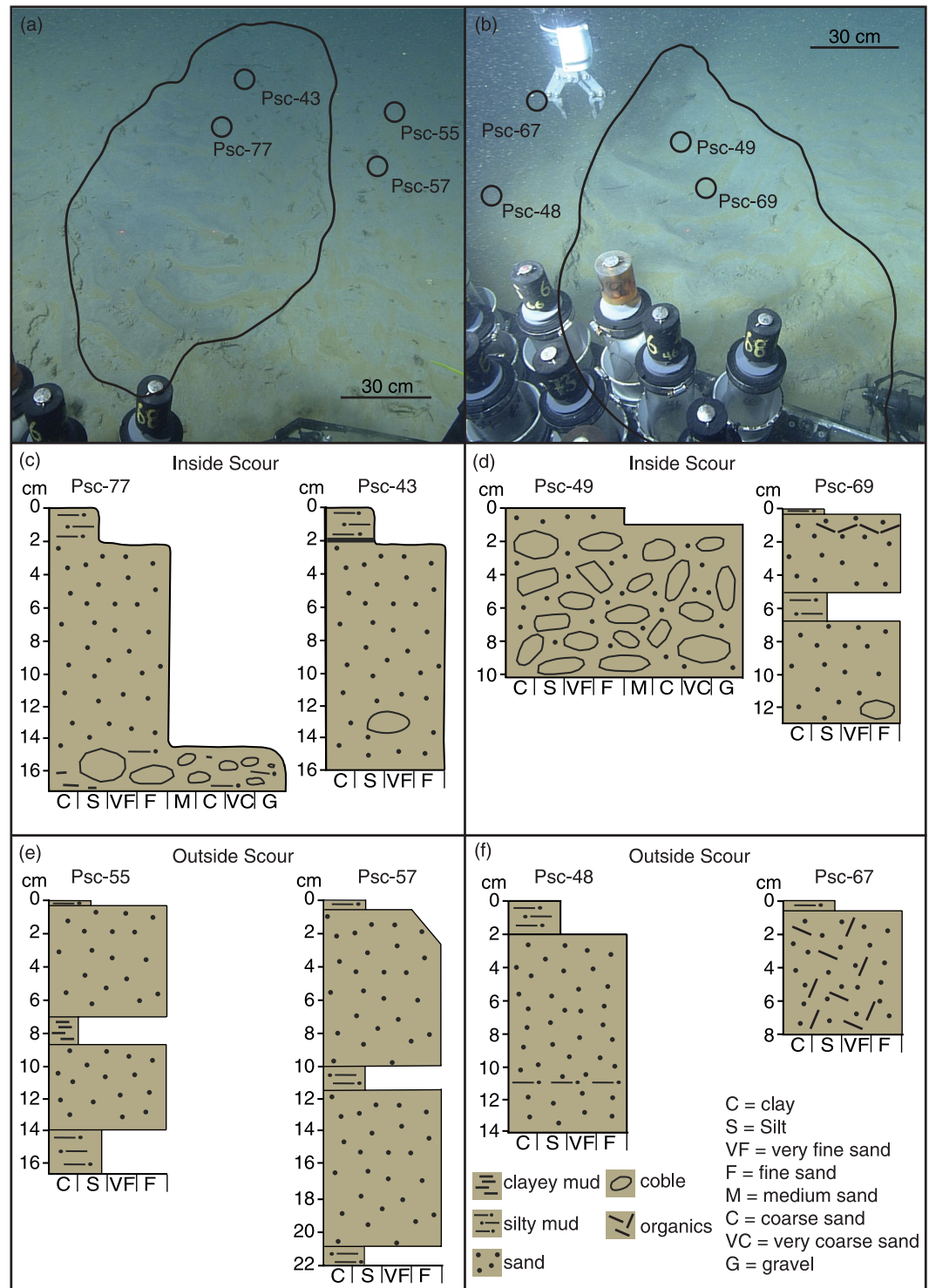


**Figure 9.** Pushcores. (a–b) Still frames from the remotely operated vehicle (ROV)-acquired video of the two scours that were sampled during the April 2017 coring cruise. Scours are outlined in black, and core locations are denoted by black circles. The tray of pushcore tubes mounted to the front of the ROV can be seen in the bottom of the images. (c–f) Pushcore descriptions.

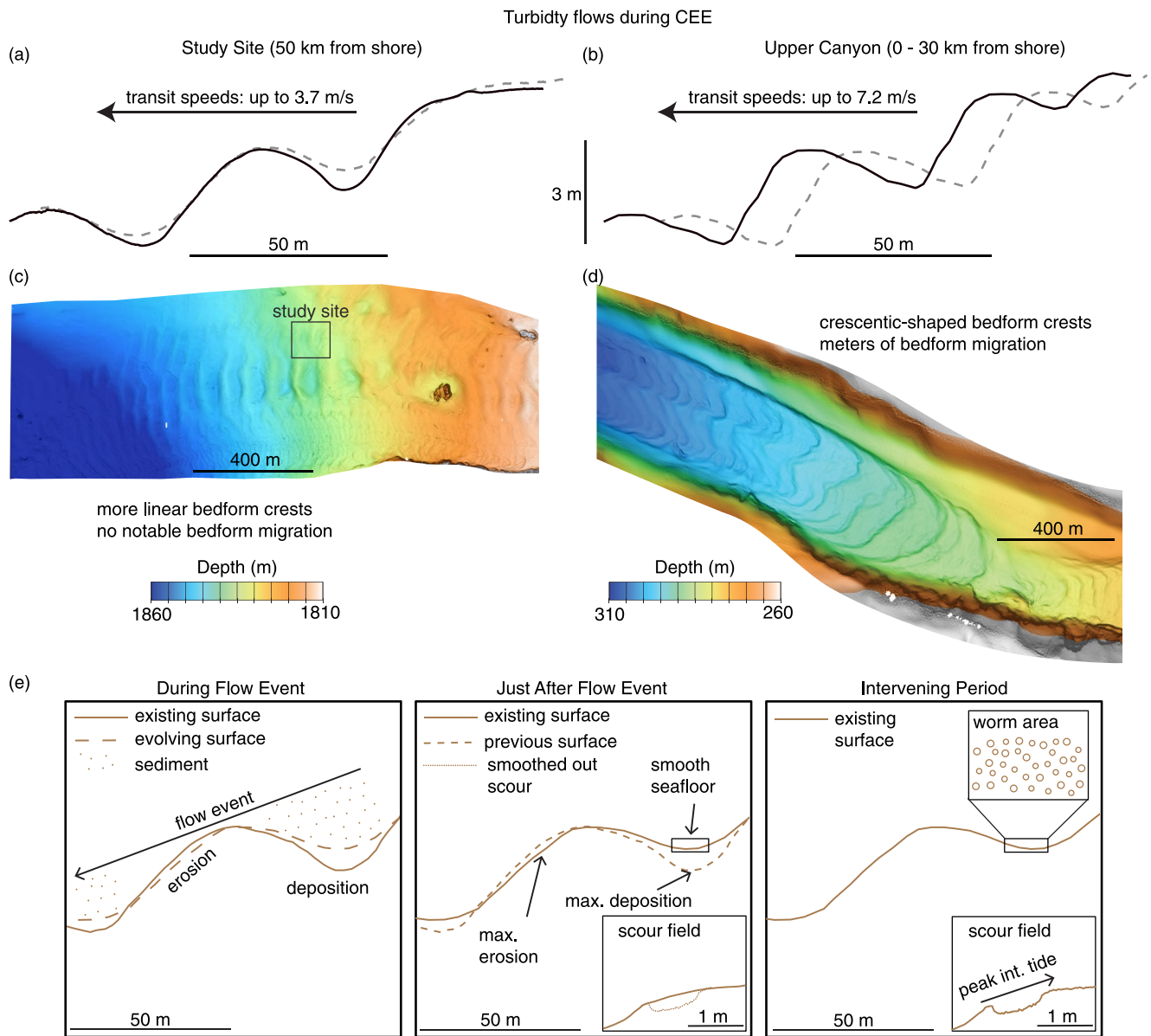


**Figure 10.** Schematic representations comparing the bedform morphology and migration within the axis of Monterey Canyon at the study site (a, c) and in upper Monterey Canyon (b, d). Bathymetry at both sites was acquired by autonomous underwater vehicles and gridded at a 1-m resolution. (e) Cartoon sketch of what happens to the seabed within the study area during, just after, and in between turbidity flow events.

interpret that the scours are then subsequently infilled and smoothed during the passage of the turbidity flows (Figure 10d). The difference in the size of the scours visible in the May 2016 and March 2017 surveys may be explained by the difference in time between the turbidity flows and the subsequent LASS survey. Excavation of the scours may also be limited to discrete periods of time, perhaps during spring tides when up-canyon internal tidal velocities exceed 0.5 m/s (Figure 7c). Why scours are not evident in the October 2016 survey, which occurred ~7 weeks after the 1 September 2016 turbidity current is unclear. Within the resolution of the surveys, the seafloor where most of these scours developed lacks obvious obstacles that could explain why the scours developed where they did (Kleinhans et al., 2017). The discontinuous ripples that make up the mottled texture extending to the northwest from the scours are presumably composed of excavated material. While internal waves/tides are thought to produce hummocky cross-stratification (Morsilli & Pomar, 2012; Pomar et al., 2012), hummocks (mounds) are not evident here. Regardless, our results show that internal tides do substantially modify the seafloor. The scale of these scours is on the order of scours preserved in the rock record (e.g., Cheel &

Middleton, 1993), providing evidence of the impact internal tides may have on the rock record, a topic that has been controversial (e.g., Shanmugam, 2014; Zhenzhong et al., 2013).

### 5.1.3. Centimeter-Scale Pits Due To Biological Activity and Recolonization

The centimeter-scale pits, observed on the northern area of freshly deposited sediment during the May 2016 survey (Figure 6c), appear to be burrows, presumably associated with polychaete worms, as suggested by ROV observations and their occurrence in pushcore samples. If the net sediment drape of 80 cm in this area was laid down at the end of the 15 January 2016 flow event, recolonization of the seabed occurred within  $\sim 117$  days. Repeat mapping at centimeter scale, therefore, can provide direct measurements of initial faunal recovery rates following seafloor disturbance.

## 5.2. Deposit Types and Their Relationship to Flow Processes

Repeat surveys document the timing of seabed aggradation (Figure 3) relative to the occurrence of turbidity currents, and thus are useful to relate deposit emplacement by specific flows. For example, the erosional discontinuity at  $\sim 60$  cm depth in core 548 (Figure 9) could represent the base of the 15 January 2016 flow deposit, which laid down at least 63 cm of sand at the core site. The slight difference in the thickness of cored deposit and measured bathymetric change may be explained by the erosion of the seabed between the bathymetric survey and the core collection ( $\sim 15$  months) and/or compaction of the core during acquisition and storage. The thinner ( $\leq 20$  cm) deposits may be associated with the weaker turbidity flows that occur later in our study period (Figure 3).

The most recent deposits sampled within the vibracores around the LASS site are broadly similar to facies described elsewhere in the canyon (Paull et al., 2005, 2010). There is little spatial variation in deposit types across the study site (Figures 8 and 9), but bedform troughs have thicker layers of finer sand than the bedform crests, as well as more abundant plant material, which is presumably sorted due to its lower density. The low-density plant material within trough-infill may be relatively easy to erode during later flows.

The internal tides seemingly excavated into sediment deposited by the recent turbidity currents to form the scours; therefore, pushcores taken inside the scours may record modern internal tidal deposits, which would be quite novel. Pushcores at one scour location indicate that there is no apparent difference in the lithology inside and outside the scours (Figures 9c and 9e). At the other scour location, however, gravel and pebbles occur near the seafloor within the scour, suggesting that the coarser lithology limited the depth to which the scouring currents were able to erode (Figures 9b and 9d). The overlying 0.5–2 cm thick mud caps probably settled after the last scouring event.

## 5.3. What Controls Bedform Type and Rate of Migration

### 5.3.1. Two Different Types of Bedform Morphology

Two distinct types of bedforms are seen in Monterey Canyon (Figures 1 and 10). The first type is the crescentic bedform that is pervasive in the upper canyon and has a steeper side that faces down-canyon (Figures 10b and 10d; also see Figure 12 in Gwiazda et al., 2022). Bedforms with a similar morphology are seen at other locations worldwide (e.g., Hage et al., 2018; Hughes Clarke, 2016; Normandeau et al., 2020, 2022; Symons et al., 2016; Wynn & Stow, 2002) where they can be linked to repeated hydraulic jumps in supercritical turbidity currents (Hughes Clarke, 2016) that may have a dense near-bed layer (Hughes Clarke, 2016; Paull et al., 2018). This study focused on a second type of bedform that is near-linear or convex down-canyon and which has a more symmetric shape with similar gradients on both sides (Figures 10a and 10c). This second type of bedform also occurs in other locations, typically where turbidity currents expand within a canyon (as in this study) or at the termination of canyons and channels (e.g., Lintern et al., 2016; Normandeau et al., 2020, 2022).

### 5.3.2. Local Comparison: Monterey Canyon

A comparison of seafloor change from time-lapse AUV surveys shows that there is far greater seabed change in the upper parts of Monterey Canyon than at the LASS site (Paull et al., 2018). The front speeds measured in all three flow events were significantly faster at sites farther up the canyon (4.8–7.2 m/s), suggesting that these flows had slowed markedly before reaching the SIN. In the period between November 2015 and January 2016, four flows were recorded in the upper canyon (Paull et al., 2018). Three of the events were confined to the upper canyon, with internal flow speeds  $\leq 5.7$  m/s. These events dissipated before reaching the second mooring, and

thus, front speeds could not be determined. The fourth event, on 15 January 2016, traversed the whole CCE instrument array, with front speeds up to 7.2 m/s in the upper canyon that then decelerated to 3.7 m/s at the LASS site (Paull et al., 2018). Pervasive seabed change of 2–3 m due to migrating bedforms occurs along much of the upper canyon during this 3 month period (Gwiazda et al., 2022; Paull et al., 2018), yet bedform crests did not migrate significantly at the LASS site, where seabed change was typically only a few 10 s of cm (Figure 10). It is striking that turbidity currents in the upper canyon carried heavy (~695 kg in water) objects for kilometers at speeds of >4 m/s, which approaches the speed of the flow front (Paull et al., 2018). In contrast, the 15 January flow moved the significantly lighter SIN (45 kg in water) for only ~26 m.

The difference in bedform migration and the size/weight of objects that move during the events may be due to the presence of dense, near-bed layers in flows in the upper canyon (Gwiazda et al., 2022; Paull et al., 2018), which dissipate by the time the flows reach the LASS site. Another factor may be that the seabed is less easily eroded at the LASS site. The upper canyon is underlain by coarse sand and pebbles that are similar to the material recovered in vibracores from the LASS area; however, the LASS area also contains significantly coarser material, including large granodiorite boulders (Paull et al., 2011), which leave them less susceptible to subsequent migration. The emplacement of the large boulders around the LASS site may be linked to the episodic occurrence of infrequent but more powerful flows than the ones observed during the CCE. It is possible that this larger scale of flow is associated with infrequent large earthquakes, as occurred in Kaikoura Canyon in 2016, where similar convex down-canyon bedforms were observed to move significantly due to an extremely large earthquake-triggered flow (see Figure 3 in Mountjoy et al., 2018).

### 5.3.3. Wider Comparison: Flow Speeds Needed for Bedform Migration at Other Sites

The 15 January 2016 flow sustained velocities >1 m/s for over an hour yet resulted in no notable bedform migration. Slower and much shorter flow events, however, have caused much greater migration of crescentic bedforms in other systems. For example, in channels cut on the Squamish Delta in Canada, turbidity currents that had maximum velocities of 1.5–2 m/s (Hage et al., 2018) or 2.5–3 m/s (Hughes Clarke, 2016) produced much greater changes to bedforms, comparable to the migration seen in the upper Monterey Canyon; despite these flows only lasting for 2–10 min. Similarly, Normandeau et al. (2020) showed how a turbidity current with internal flow speeds of 2 m/s caused substantial upslope bedform migration in a study from Pointe-des-Monts in the Gulf of Saint Lawrence.

The observation that more prolonged and faster flows at the LASS site in Monterey Canyon during the CCE cause less bedform migration and seabed change than slower and shorter turbidity currents at other sites is surprising. The channels offshore Squamish Delta are underlain by sand-dominated deposits with occasional clasts (see Figure 3 in Hage et al., 2018), which are broadly comparable to deposits cored by this study (Figures 8 and 9) and to those in the upper parts of Monterey Canyon (Paull et al., 2005, 2010). However, they appear to lack the large boulders observed in and around the LASS study area. These observations lend credence to the hypothesis that the lack of migration at the LASS site may be due, at least in part, to lower erodibility of the underlying sediment as the large boulders act to anchor the bedforms. Relatedly, some depositional processes during turbidity flows (e.g., cyclic steps) may produce loosely packed sands that are more easily eroded and reworked.

Where bedform migration occurs during weaker or shorter flows, the bedforms have distinctive up-canyon convex (crescentic) crests similar to those in upper Monterey Canyon (e.g., Hage et al., 2018; Hughes Clarke, 2016; Normandeau et al., 2020, 2022; Symons et al., 2016; Wynn & Stow, 2002). Squamish Delta monitoring shows that movement of these bedforms may be linked to dense near-bed layers and cyclic steps in faster and supercritical flows (Hughes Clarke, 2016). These observations suggest that bedform migration is much greater when dense near-bed layers are present within the flows, further suggesting that these near-bed layers were absent or diminished by the time flows in Monterey Canyon reached the SIN. Whatever the cause, faster and more prolonged turbidity currents can produce less bedform migration than weaker and shorter-lived flows, despite both producing deposits of sand and pebbles.

Finally, it is notable that despite causing no bedform migration, the 15 January 2016 flow moved the 45 kg (in water) SIN for ~26 m down canyon. A similar observation comes from the Fraser Delta offshore Vancouver in Canada, where a powerful turbidity current (with internal speeds of 6.75–9 m/s) carried a 1,100 kg (in water) benthic instrument frame downslope up to 75 m, without causing seabed change that could be resolved from ship-based multibeam surveys (>30–70 cm; Lintern et al., 2016). This open-slope location on the Fraser Delta has more linear or reverse-crested bedforms resembling those at the LASS site, rather than the crescentic-shaped bedforms associated with supercritical flows in upper Monterey Canyon and elsewhere. Thus, it is possible that relatively powerful but sub-critical turbidity currents, which also lack dense near-bed layers, may cause relatively small change to the seabed.

## 6. Conclusions

The new Low-Altitude Survey System (LASS) system provides the first repeat cm-scale mapping of submarine canyons in the deep sea, illustrating how novel technology can advance mapping capabilities in such remote settings. Repeat (time-lapse) ultra-high-resolution mapping of a 20,000 m<sup>3</sup> area of Monterey Canyon at ~1,840 m water depth was combined with detailed monitoring of active current flows and precise seabed coring. This combined information is used to understand how three turbidity currents with flow speeds of up to 3.3 m/s, and somewhat weaker (up to 0.7 m/s) internal tides, modified the canyon floor and deposited sediment over an 18-month period.

Two different types of bedform morphology are observed in Monterey Canyon. The first type of “crescentic” bedforms are pervasive in the upper canyon and are linked to repeated hydraulic jumps in supercritical turbidity currents, which likely have dense near-bed layers. Here we studied a second type of “reverse curvature” bedform with near-linear or convex down-canyon crests and a more symmetric profile shape. The reverse curvature bedforms are associated with a widening of the channel axis in Monterey Canyon and the lateral expansion of turbidity currents in other settings.

Three relatively fast (0.9–3.3 m/s) and prolonged (up to 112 min) turbidity currents failed to cause significant movement of these reverse curvature bedforms in Monterey Canyon. This is surprising given that turbidity currents with comparable speeds (m/s) produce rapid migration of crescentic bedforms in upper Monterey Canyon and at other sites worldwide. Migration rates of the reverse curvature bedforms at the study site may be controlled by the character of the substrate sediment. Large, granodiorite boulders that outcrop along the crests of these bedforms suggest that the bedforms are underlain with extremely coarse material, which may anchor against migration during the observed flows. The lack of significant migration may also indicate that turbidity currents no longer contain dense near-bed layers by the time they reach the Seafloor Instrument Node (SIN).

The LASS surveyed two fields of seabed scours, several centimeters to meters in length and width, and tens of centimeters deep, with internal 1-cm ribbing. These features elongate in the direction of the upcanyon internal tides. Ultra-high resolution bathymetric observations combined with the continuous flow monitoring, have, for the first time, shown that scours on channel beds and internal tides may be causally related. Internal tides may also help to infill the troughs between reverse curvature bedforms. Thus, this study starts to test how internal tides may produce features recorded in the ancient rock record.

This paper illustrates how new technologies for ultra-high-resolution mapping can produce greater understanding of seabed processes, especially when combined with flow monitoring and cores. The centimeter-scale resolution of the LASS bathymetry has revealed features never before seen in such striking detail. The spatial scale of this new seabed mapping approaches that of observations in ancient rock outcrops, showing how a current gap between field studies and the rock record may eventually be bridged.

## Conflict of Interest

The authors declare no conflicts of interest relevant to this study.

## Data Availability Statement

The processed and gridded lidar and multibeam bathymetry data used in this study are available at Zenodo.org: ROV cm-scale seafloor surveys at 1,840 m depth in Monterey Canyon, via <https://doi.org/10.5281/zenodo.6071543>. Data are open-access and licensed with Creative Commons Attribution 4.0 International (Wolfson-Schwehr et al., 2022). Version 5.7.6 of MB-System, used for the processing and gridding of the bathymetry data, as well as the photomosaicing of the stereo imagery, is preserved in a GitHub repository via <https://github.com/dwcaress/MB-System/releases/5.7.6>. The software is open-source and licensed with GNU General Public License, version 3 (Caress et al., 2020).

### Acknowledgments

Support for this research was provided by the David and Lucile Packard Foundation and the Natural Environment Research Council (NE/K011480/1). The authors are very appreciative of the crews of the R/Vs *Western Flyer* and *Rachel Carson*, the pilots of the ROV *Doc Ricketts*, and the AUV operators. The authors would also like to thank reviewers at the USGS Pacific Coastal and Marine Science Center, including Kurt Rosenberger, as well as anonymous reviewers for the journal, whose constructive feedback helped to significantly improve this manuscript. Any use of trade, firm, or product names is for descriptive purposes only and does not imply endorsement by the U.S. government.

### References

- Bailey, L. P., Clare, M. A., Rosenberger, K. J., Cartigny, M. J. B., Talling, P. J., Paull, C. K., et al. (2021). Preconditioning by sediment accumulation can produce powerful turbidity currents without major external triggers. *Earth and Planetary Science Letters*, *562*, 116845. <https://doi.org/10.1016/j.epsl.2021.116845>
- Bruschi, R., Bughi, S., Spinazze, M., Torselletti, E., & Vitali, L. (2006). Impact of debris flows and turbidity currents on seafloor structures. *Nowegian Journal of Geology*, *86*, 317–336.
- Canals, M., Puig, P., de Madron, X. D., Heussner, S., Palanques, A., & Fabres, J. (2006). Flushing submarine canyons. *Nature*, *444*(7117), 354–357. <https://doi.org/10.1038/nature05271>
- Caress, D. W., & Chayes, D. N. (1996). Improved processing of hydrosweep DS multibeam data on the R/V Maurice Ewing. *Marine Geophysical Researches*, *18*(6), 631–650. <https://doi.org/10.1007/BF00313878>
- Caress, D. W., Chayes, D. N., & dos Ferreira, C. S. (2020). MB-system (version 5.7.6) [Software]. Retrieved from <https://github.com/dwcaress/MB-System/releases/5.7.6>
- Caress, D. W., Clague, D. A., Paduan, J. B., Martin, J. F., Dreyer, B. M., Chadwick, W. W., et al. (2012). Repeat bathymetric surveys at 1-metre resolution of lava flows erupted at Axial Seamount in April 2011. *Nature Geoscience*, *5*(7), 483–488. <https://doi.org/10.1038/ngeo1496>
- Carter, L., Gavey, R., Talling, P., & Liu, J. (2014). Insights into submarine geohazards from breaks in subsea telecommunication cables. *Oceanography*, *27*(2), 58–67. <https://doi.org/10.5670/oceanog.2014.40>
- Cheel, R. J., & Middleton, G. V. (1993). Directional scours on a transgressive surface: Examples from the Silurian Whirlpool Sandstone of southern Ontario, Canada. *Journal of Sedimentary Petrology*, *63*(3), 392–397.
- De Leo, F. C., & Puig, P. (2018). Bridging the gap between the shallow and deep oceans: The key role of submarine canyons. *Progress in Oceanography*, *169*, 1–5. <https://doi.org/10.1016/j.pocan.2018.08.006>
- Fox, C. G., Chadwick, W. W., & Embley, R. W. (1992). Detection of changes in ridge-crest morphology using repeated multibeam sonar surveys. *Journal of Geophysical Research*, *97*(B7), 11149–11162. <https://doi.org/10.1029/92JB00601>
- Fujiwara, T., Kodaira, S., No, T., Kaiho, Y., Takahashi, N., & Kaneda, Y. (2011). The 2011 Tohoku-Oki earthquake: Displacement reaching the trench axis. *Science*, *334*(6060), 1240. <https://doi.org/10.1126/science.1211554>
- Galy, V., France-Lanord, C., Beyssac, O., Faure, P., Kudrass, H., & Palhol, F. (2007). Efficient organic carbon burial in the Bengal fan sustained by the Himalayan erosional system. *Nature*, *450*(7168), 407–410. <https://doi.org/10.1038/nature06273>
- Gwiazda, R., Paull, C. K., Kieft, B., Klimov, D., Herlien, R., Lundsten, E., et al. (2022). Near-bed structure of sediment gravity flows measured by motion-sensing “boulder-like” benthic event detectors (BEDs) in Monterey Canyon. *Journal of Geophysical Research: Earth Surface*, *127*(2), e2021JF006437. <https://doi.org/10.1029/2021JF006437>
- Hage, S., Cartigny, M. J. B., Clare, M. A., Sumner, E. J., Vendettuoli, D., Hughes Clarke, J. E., et al. (2018). How to recognize crescentic bedforms formed by supercritical turbidity currents in the geologic record: Insights from active submarine channels. *Geology*, *46*(6), 563–566. <https://doi.org/10.1130/G40095.1>
- Hall, R. A., & Carter, G. S. (2011). Internal tides in Monterey submarine canyon. *Journal of Physical Oceanography*, *41*(1), 186–204. <https://doi.org/10.1175/2010JPO4471.1>
- Heerema, C. J., Talling, P. J., Cartigny, M. J., Paull, C. K., Bailey, L., Simmons, S. M., et al. (2020). What determines the downstream evolution of turbidity currents? *Earth and Planetary Science Letters*, *532*, 116023. <https://doi.org/10.1016/j.epsl.2019.116023>
- Heijnen, M. S., Clare, M. A., Cartigny, M. J. B., Talling, P. J., Hage, S., Lintern, D. G., et al. (2020). Rapidly-migrating and internally-generated knickpoints can control submarine channel evolution. *Nature Communications*, *11*(1), 3129. <https://doi.org/10.1038/s41467-020-16861-x>
- Hughes Clarke, J. E. (2016). First wide-angle view of channelized turbidity currents links migrating cyclic steps to flow characteristics. *Nature Communications*, *7*(1), 1–13. <https://doi.org/10.1038/ncomms11896>
- Key, S. A. (1999). *Internal tidal bores in the Monterey Canyon* (M.S. Thesis). Naval Postgraduate School.
- Kleinans, M. G., Leuven, J. R. F. W., Braat, L., & Baar, A. (2017). Scour holes and ripples occur below the hydraulic smooth to rough transition of movable beds. *Sedimentology*, *64*(5), 1381–1401. <https://doi.org/10.1111/sed.12358>
- Kunze, E., Rosenfeld, L. K., Carter, G. S., & Gregg, M. C. (2002). Internal waves in Monterey submarine canyon. *Journal of Physical Oceanography*, *32*(6), 1890–1913. [https://doi.org/10.1175/1520-0485\(2002\)032<1890:IWMSC>2.0.CO;2](https://doi.org/10.1175/1520-0485(2002)032<1890:IWMSC>2.0.CO;2)
- Lintern, D. G., Hill, P. R., & Stacey, C. (2016). Powerful unconfined turbidity current captured by cabled observatory on the Fraser River delta slope, British Columbia, Canada. *Sedimentology*, *63*(5), 1041–1064. <https://doi.org/10.1111/sed.12262>
- Maier, K. L., Gales, J. A., Paull, C. K., Rosenberger, K., Talling, P. J., Simmons, S. M., et al. (2019). Linking direct measurements of turbidity currents to submarine canyon-floor deposits. *Frontiers of Earth Science*, *7*, 144. <https://doi.org/10.3389/feart.2019.00144>
- Miner, M. D., Kulp, M. A., FitzGerald, D. M., & Georgiou, I. Y. (2009). Hurricane-associated ebb-tidal delta sediment dynamics. *Geology*, *37*(9), 851–854. <https://doi.org/10.1130/G25466A.1>
- Morsilli, M., & Pomar, L. (2012). Internal waves vs. surface storm waves: A review on the origin of hummocky cross-stratification. *Terra Nova*, *24*(4), 273–282. <https://doi.org/10.1111/j.1365-3121.2012.01070.x>
- Mountjoy, J. J., Howarth, J. D., Orpin, A. R., Barnes, P. M., Bowden, D. A., Rowden, A. A., et al. (2018). Earthquakes drive large-scale submarine canyon development and sediment supply to deep-ocean basins. *Science Advances*, *4*(3), eaar3748. <https://doi.org/10.1126/sciadv.aar3748>
- Normandeau, A., Bourgault, D., Neumeier, U., Lajeunesse, P., St-Onge, G., Gostiaux, L., & Chavanne, C. (2020). Storm-induced turbidity currents on a sediment-starved shelf: Insight from direct monitoring and repeat seabed mapping of upslope migrating bedforms. *Sedimentology*, *67*(2), 1045–1068. <https://doi.org/10.1111/sed.12673>
- Normandeau, A., Lajeunesse, P., Ghienne, J.-F., & Dietrich, P. (2022). Detailed seafloor imagery of turbidity current bedforms reveals new insight into fine-scale near-bed processes. *Geophysical Research Letters*, *49*(11), e2021GL097389. <https://doi.org/10.1029/2021GL097389>
- Paull, C. K., Caress, D. W., Ussler, W., Lundsten, E., & Meiner-Johnson, M. (2011). High-resolution bathymetry of the axial channels within Monterey and Soquel submarine canyons, offshore central California. *Geosphere*, *7*(5), 1077–1101. <https://doi.org/10.1130/GES00636.1>
- Paull, C. K., Iii, W. U., Caress, D. W., Lundsten, E., Covault, J. A., Maier, K. L., et al. (2010). Origins of large crescent-shaped bedforms within the axial channel of Monterey Canyon, offshore California. *Geosphere*, *6*(6), 755–774. <https://doi.org/10.1130/GES00527.1>
- Paull, C. K., Mitts, P., Ussler, W., Keaten, R., & Greene, H. G. (2005). Trail of sand in upper Monterey Canyon: Offshore California. *GSA Bulletin*, *117*(9–10), 1134–1145. <https://doi.org/10.1130/B25390.1>
- Paull, C. K., Talling, P. J., Maier, K. L., Parsons, D., Xu, J., Caress, D. W., et al. (2018). Powerful turbidity currents driven by dense basal layers. *Nature Communications*, *9*(4114), 9. <https://doi.org/10.1038/s41467-018-06254-6>
- Peakall, J., Best, J., Baas, J. H., Hodgson, D. M., Clare, M. A., Talling, P. J., et al. (2020). An integrated process-based model of flutes and tool marks in deep-water environments: Implications for palaeohydraulics, the Bouma sequence and hybrid event beds. *Sedimentology*, *67*(4), 1601–1666. <https://doi.org/10.1111/sed.12727>

- Petruncio, E. T., Rosenfeld, L. K., & Paduan, J. D. (1998). Observations of the internal tide in Monterey Canyon. *Journal of Physical Oceanography*, 28(10), 1873–1903. [https://doi.org/10.1175/1520-0485\(1998\)028<1873:OOTITI>2.0.CO;2](https://doi.org/10.1175/1520-0485(1998)028<1873:OOTITI>2.0.CO;2)
- Pomar, L., Morsilli, M., Hallock, P., & Bádenas, B. (2012). Internal waves, an under-explored source of turbulence events in the sedimentary record. *Earth-Science Reviews*, 111(1), 56–81. <https://doi.org/10.1016/j.earscirev.2011.12.005>
- Roman, C., & Mather, R. (2010). Autonomous underwater vehicles as tools for deep-submergence archaeology. *Proceedings of the Institution of Mechanical Engineers - Part M: Journal of Engineering for the Maritime Environment*, 224(4), 327–340. <https://doi.org/10.1243/14750902JEME202>
- Shanmugam, G. (2014). Review of research in internal-wave and internal-tide deposits of China: Discussion. *Journal of Palaeogeography*, 3(4), 332–350. <https://doi.org/10.3724/SP.J.1261.2014.00060>
- Smith, D. P., Ruiz, G., Kvitek, R., & Iampietro, P. J. (2005). Semiannual patterns of erosion and deposition in upper Monterey Canyon from serial multibeam bathymetry. *GSA Bulletin*, 117(9–10), 1123–1133. <https://doi.org/10.1130/B25510.1>
- Symons, W. O., Sumner, E. J., Paull, C. K., Xu, J. P., Maier, K. L., Lorenson, T. D., & Talling, P. J. (2017). A new model for turbidity current behavior based on integration of flow monitoring and precision coring in a submarine canyon. *Geology*, 45(4), 367–370. <https://doi.org/10.1130/G38764.1>
- Symons, W. O., Sumner, E. J., Talling, P. J., Cartigny, M. J. B., & Clare, M. A. (2016). Large-scale sediment waves and scours on the modern seafloor and their implications for the prevalence of supercritical flows. *Marine Geology*, 371, 130–148. <https://doi.org/10.1016/j.margeo.2015.11.009>
- Weimer, P., & Link, M. H. (1991). Global petroleum occurrences in submarine fans and turbidite systems. In P. Weimer & M. H. Link (Eds.), *Seismic facies and sedimentary processes of submarine fans and turbidite systems* (pp. 9–67). Springer. [https://doi.org/10.1007/978-1-4684-8276-8\\_2](https://doi.org/10.1007/978-1-4684-8276-8_2)
- Wolfson-Schwehr, M., Caress, D. W., Paull, C. K., Thomas, H., Martin, E., Troni, G., et al. (2022). ROV cm-scale seafloor surveys at 1840 m depth in Monterey Canyon (Version 1.0.1) [Dataset]. Zenodo. <https://doi.org/10.5281/zenodo.6071543>
- Wynn, R. B., & Stow, D. A. V. (2002). Classification and characterisation of deep-water sediment waves. *Marine Geology*, 192(1), 7–22. [https://doi.org/10.1016/S0025-3227\(02\)00547-9](https://doi.org/10.1016/S0025-3227(02)00547-9)
- Xu, J. P., & Noble, M. A. (2009). Currents in Monterey submarine canyon. *Journal of Geophysical Research*, 114(C3), C03004. <https://doi.org/10.1029/2008JC004992>
- Xu, J. P., Noble, M. A., & Rosenfeld, L. K. (2004). In situ measurements of velocity structure within turbidity currents. *Geophysical Research Letters*, 31(9), 4. <https://doi.org/10.1029/2004GL019718>
- Xu, J. P., Wong, F. L., Kvitek, R., Smith, D. P., & Paull, C. K. (2008). Sandwave migration in Monterey submarine canyon, Central California. *Marine Geology*, 248(3), 193–212. <https://doi.org/10.1016/j.margeo.2007.11.005>
- Zhenzhong, G., Youbin, H., Xiangdong, L., Taizhong, D., Yuan, W., & Min, L. (2013). Review of research in internal-wave and internal-tide deposits of China. *Journal of Palaeogeography*, 2(1), 56–65. <https://doi.org/10.3724/SP.J.1261.2013.00017>

## References From the Supporting Information

- Carter, L., Milliman, J. D., Talling, P. J., Gavey, R., & Wynn, R. B. (2012). Near-synchronous and delayed initiation of long run-out submarine sediment flows from a record-breaking river flood, offshore Taiwan. *Geophysical Research Letters*, 39(12), L12603. <https://doi.org/10.1029/2012GL051172>
- Gavey, R., Carter, L., Liu, J. T., Talling, P. J., Hsu, R., Pope, E., & Evans, G. (2017). Frequent sediment density flows during 2006 to 2015, triggered by competing seismic and weather events: Observations from subsea cable breaks off southern Taiwan. *Marine Geology*, 384, 147–158. <https://doi.org/10.1016/j.margeo.2016.06.001>
- Heijnen, M. S., Mienis, F., Gates, A. R., Bett, B. J., Hall, R. A., Hunt, J., et al. (2022). Challenging the highstand-dormant paradigm for land-detached submarine canyons. *Nature Communications*, 13(1), 3448. <https://doi.org/10.1038/s41467-022-31114-9>
- Khripounoff, A., Vangriesheim, A., Babonneau, N., Crassous, P., Dennielou, B., & Savoye, B. (2003). Direct observation of intense turbidity current activity in the Zaire submarine valley at 4000 m water depth. *Marine Geology*, 194(3), 151–158. [https://doi.org/10.1016/S0025-3227\(02\)00677-1](https://doi.org/10.1016/S0025-3227(02)00677-1)
- Khripounoff, A., Vangriesheim, A., Crassous, P., & Etoubleau, J. (2009). High frequency of sediment gravity flow events in the Var submarine canyon (Mediterranean Sea). *Marine Geology*, 263(1), 1–6. <https://doi.org/10.1016/j.margeo.2009.03.014>
- Liu, J. T., Hsu, R. T., Hung, J.-J., Chang, Y.-P., Wang, Y.-H., Rendle-Bühning, R. H., et al. (2016). From the highest to the deepest: The Gaoping River–Gaoping Submarine Canyon dispersal system. *Earth-Science Reviews*, 153, 274–300. <https://doi.org/10.1016/j.earscirev.2015.10.012>
- Simmons, S. M., Azpiroz-Zabala, M., Cartigny, M. J. B., Clare, M. A., Cooper, C., Parsons, D. R., et al. (2020). Novel acoustic method provides first detailed measurements of sediment concentration structure within submarine turbidity currents. *Journal of Geophysical Research: Oceans*, 125(5), e2019JC015904. <https://doi.org/10.1029/2019JC015904>
- Talling, P. J., Baker, M. L., Pope, E. L., Ruffell, S. C., Jacinto, R. S., Heijnen, M. S., et al. (2022). Longest sediment flows yet measured show how major rivers connect efficiently to deep sea. *Nature Communications*, 13(1), 4193. <https://doi.org/10.1038/s41467-022-31689-3>
- Wang, Z., Xu, J., Talling, P. J., Cartigny, M. J. B., Simmons, S. M., Gwiazda, R., et al. (2020). Direct evidence of a high-concentration basal layer in a submarine turbidity current. *Deep Sea Research Part I: Oceanographic Research Papers*, 161, 103300. <https://doi.org/10.1016/j.dsr.2020.103300>
- Xu, J. P., Swarzenski, P. W., Noble, M., & Li, A.-C. (2010). Event-driven sediment flux in Hueneme and Mugu submarine canyons, southern California. *Marine Geology*, 269(1), 74–88. <https://doi.org/10.1016/j.margeo.2009.12.007>